A seasonal trend of single scattering albedo in southern African biomass-burning particles: Implications for satellite products and estimates of emissions for the world's largest biomass-burning source

T. F. Eck,[1,2] B. N. Holben,[2] J. S. Reid,[3] M. M. Mukelabai,[4] S. J. Piketh,[5] O. Torres,[2] H. T. Jethva,[1,2] E. J. Hyer,[3] D. E. Ward,[6] O. Dubovik,[7] A. Sinyuk,[2,8] J. S. Schafer,[2,8] D. M. Giles,[2,8] M. Sorokin,[2,8] A. Smirnov,[2,8] and I. Slutsker[2,8]

Received 19 February 2013; revised 10 May 2013; accepted 16 May 2013; published 19 June 2013.

[1] As a representative site of the southern African biomass-burning region, sun-sky data from the 15 year Aerosol Robotic Network (AERONET) deployment at Mongu, Zambia, was analyzed. For the biomass-burning season months (July–November), we investigate seasonal trends in aerosol single scattering albedo (SSA), aerosol size distributions, and refractive indices from almucantar sky scan retrievals. The monthly mean single scattering albedo at 440 nm in Mongu was found to increase significantly from ~0.84 in July to ~0.93 in November (from 0.78 to 0.90 at 675 nm in these same months). There was no significant change in particle size, in either the dominant accumulation or secondary coarse modes during these months, nor any significant trend in the Ångström exponent (440–870 nm; $r^2 = 0.02$). A significant downward seasonal trend in imaginary refractive index ($r^2 = 0.43$) suggests a trend of decreasing black carbon content in the aerosol composition as the burning season progresses. Similarly, burning season SSA retrievals for the Etosha Pan, Namibia AERONET site also show very similar increasing single scattering albedo values and decreasing imaginary refractive index as the season progresses. Furthermore, retrievals of SSA at 388 nm from the Ozone Monitoring Instrument satellite sensor show similar seasonal trends as observed by AERONET and suggest that this seasonal shift is widespread throughout much of southern Africa. A seasonal shift in the satellite retrieval bias of aerosol optical depth from the Moderate Resolution Imaging Spectroradiometer collection 5 dark target algorithm is consistent with this seasonal SSA trend since the algorithm assumes a constant value of SSA. Multi-angle Imaging Spectroradiometer, however, appears less sensitive to the absorption-induced bias.

Citation: Eck, T. F., et al. (2013), A seasonal trend of single scattering albedo in southern African biomass-burning particles: Implications for satellite products and estimates of emissions for the world's largest biomass-burning source, *J. Geophys. Res. Atmos.*, *118*, 6414–6432, doi:10.1002/jgrd.50500.

1. Introduction

[2] Southern Africa has consistently been identified as the world's largest single source of biomass-burning emissions [*Crutzen and Andreae*, 1990; *Giglio et al.*, 2003a, 2006, 2010; *Reid et al.*, 2009; *van der Werf et al.*, 2010], and therefore, this region is important to any global budget of greenhouse gas, aerosol, or black carbon emissions. A topic of critical importance to aerosol research in this region is particle light absorption. Aerosol spectral absorption has been measured at numerous sites globally in a consistent manner by sun-sky radiometers in the Aerosol Robotic Network (AERONET) [*Holben et al.*, 1998; *Dubovik et al.*, 2002] using common calibration and data processing procedures. Among the most absorbing aerosol particles (lowest single scattering albedo (SSA)) measured at any AERONET sites are those occurring during the biomass-burning season in Zambia in the southern Africa savanna-burning region [*Dubovik et al.*, 2002; *Giles et al.*, 2012]. This results from the relatively high fraction of flaming versus smoldering combustion that occurs during grass burning in the savanna environment, compared to the larger fraction of smoldering combustion of woody fuels in some other environments, as

[1]Universities Space Research Association, Columbia, Maryland, USA.
[2]NASA Goddard Space Flight Center, Greenbelt, Maryland, USA.
[3]Naval Research Laboratory, Monterey, California, USA.
[4]Zambian Meteorological Department, Lusaka, Zambia.
[5]School of Geo- and Spatial Sciences, North-West University, Potchefstroom, South Africa.
[6]Enviropyronics, White Salmon, Washington, USA.
[7]Universite de Lille, Villeneuve d'Ascq, France.
[8]Sigma Space Corporation, Lanham, Maryland, USA.

Corresponding author: T. F. Eck, NASA Goddard Space Flight Center, Code 618, Greenbelt, MD 20771, USA. (thomas.f.eck@nasa.gov)

2169-897X/13/10.1002/jgrd.50500

had been measured in situ during controlled burns by *Ward et al*. [1992, 1996].

[3] From a climate point of view, aerosol absorption is a key parameter affecting the aerosol direct radiative forcing at the top of the atmosphere, solar radiation incident at the surface, and radiative heating of the aerosol layer. All of these impacts have significant consequences on atmospheric stability and perhaps clouds through the semidirect effect [*Pilinis et al*., 1995; *IPCC*, 2007]. Seasonal variation of spectral SSA has been observed to occur at some AERONET sites (Kanpur, India; Beijing, China; and Ilorin, Nigeria) where there are varying mixtures of fine- and coarse-mode aerosol particles [*Eck et al*., 2010], with the relative abundance of the two distinct aerosol types (i.e., desert dust and pollution or smoke) driving much of the annual variation. Additionally, a multiyear trend in aerosol absorption was detected at Beijing with AERONET retrieved SSA by *Lyapustin et al*. [2011], made possible by the very high aerosol optical depths (AODs) at that site, since the sensitivity to absorption increases significantly as AOD increases. These results indicate that perhaps using a fixed SSA value may lead to uncertainty in forcing calculations at some locations.

[4] For southern Africa, with its significant smoke particle sources, high AOD, low particle SSA, and sometimes complex coastal stratocumulus cloud patterns, we would expect a significant impact of aerosol particles on the atmosphere. However, a wide variety of assumptions can be made regarding particle properties such as SSA to help parameterize absorption. For example, recently, *Chand et al*. [2009], *Sakaeda et al*. [2011], and *Wilcox* [2012] have estimated the direct and semidirect radiative forcing of biomass-burning aerosols over stratocumulus clouds off of the western tropical Atlantic coast of Africa (equator to 20°S in *Wilcox* [2012]; 10°N–30°S in *Sakaeda et al*. [2011]; 7.5°S–22.5°S in *Chand et al*. [2009]). The columnar weighted SSA computed by *Sakaeda et al*. [2011] ranged from ~0.97 to 0.86. This wide range of computed SSA values is partly the result of a variability of aerosol species other than carbonaceous species included in their model. On the other hand, *Wilcox* [2012] assumed a constant SSA value of 0.89 at 550 nm for the months of July–September, while Chand assumed a constant value of 0.85 in the midvisible for July–October. Diversity in assumed SSA values such as reported here translates to community-wide uncertainty in the effects of aerosol particles in the regional climate, particularly for cases of aerosol particles over clouds where the impact of aerosol absorption is enhanced.

[5] A second area of importance of aerosol absorption and SSA is in the sensitivities of some satellite AOD retrievals. Particle absorption, particularly in multiple scattering environments (say $\mathrm{AOD} > 0.5$), plays an increasingly important role in top of atmosphere (TOA) radiances used by satellites to infer AOD. Some satellite algorithms such as for the Moderate Resolution Imaging Spectroradiometer (MODIS) collection 5 (C5) over land algorithm assume regional SSAs in their calculations [*Levy et al*., 2007a, 2007b], while products such as from the Multi-angle Imaging Spectroradiometer (MISR) algorithm [*Kahn et al*., 2010] try to account for the impact of varying absorption on retrieved AOD. *Robles-Gonzalez and de Leeuw* [2008] presented a satellite retrieval algorithm utilizing ATSR-2 data that attempted to account for changes in aerosol absorption. This algorithm was applied to data over southern Africa; however, they concluded that aerosol properties were not accurately retrieved for strongly absorbing aerosols resulting from biomass burning. More recently, *Holzer-Popp et al*. [2013] discuss several satellite retrieval algorithms developed for application to European Earth observation satellite sensor data, some of which account for variation in aerosol absorption properties.

[6] With its high and consistent aerosol signal, the Mongu site in southern Africa has been a widely utilized location to verify satellite aerosol products. Indeed, it is the only long-term AERONET site with proximity to the south African smoke plume, and many AOD verification studies are highly dependent on that particular site. For example, *Ichoku et al*. [2003] found that the previously assumed regional SSA value for southern Africa of 0.90 in early MODIS retrievals for this region resulted in significant underestimates of AOD from the MODIS sensor, especially at high AOD, while an assumed value of 0.87 at 470 nm would have yielded much more accurate values. Even after iteration, the current MODIS C5 still retains a substantial regional low bias, attributed to error in absorption assumptions [*Hyer et al*., 2011]. *Kahn et al*. [2010] also included performance metrics of MISR to the southern African biomass-burning plume using data from Mongu as a representative site.

[7] In early analysis of the Mongu AERONET site, it was noticed that the southern African smoke plume single scattering albedo exhibits a significant and robust seasonal cycle. This led to questions on the cycle's implications for both smoke radiative forcing and on satellite AOD retrievals in the world's largest smoke source. By extension, there are then further questions regarding attempts to invert smoke emissions from satellite data. In this paper, we will focus on the seasonal variation of aerosol absorption at AERONET sites in the southern Africa region during the biomass-burning season of July to November [*Swap et al*., 2003]. In the first part, we describe the nature of seasonal variability in smoke single scattering albedo at the Mongu site. In the second part, we examine the implications of variability in single scattering albedo in satellite aerosol products, such as in aforementioned MODIS and MISR retrievals of AOD. In addition, we examine recent algorithms that have been developed to retrieve aerosol SSA from satellite-measured UV radiances [*Torres et al*., 2005; *Jethva and Torres*, 2011]. We conclude with a discussion on the implications of our findings on aerosol radiative forcing and inverse modeling estimates of the smoke source magnitude.

2. Instrumentation, Study Sites, Data, and Techniques

2.1. Study Region and AERONET Sites

[8] A map showing the locations of the AERONET sun-sky radiometers utilized in this study is shown in Figure 1a. The principal AERONET site analyzed in this study is the Mongu, Zambia site (15°15′S; 23°09′E) located in western Zambia and selected to characterize the biomass-burning aerosols in this region of extensive savanna burning (note numerous fire counts in Figure 1b). The data set at Mongu is one of the longest and most complete sets of aerosol optical properties measurements made at any site in the AERONET network, beginning in June 1995 and continuing

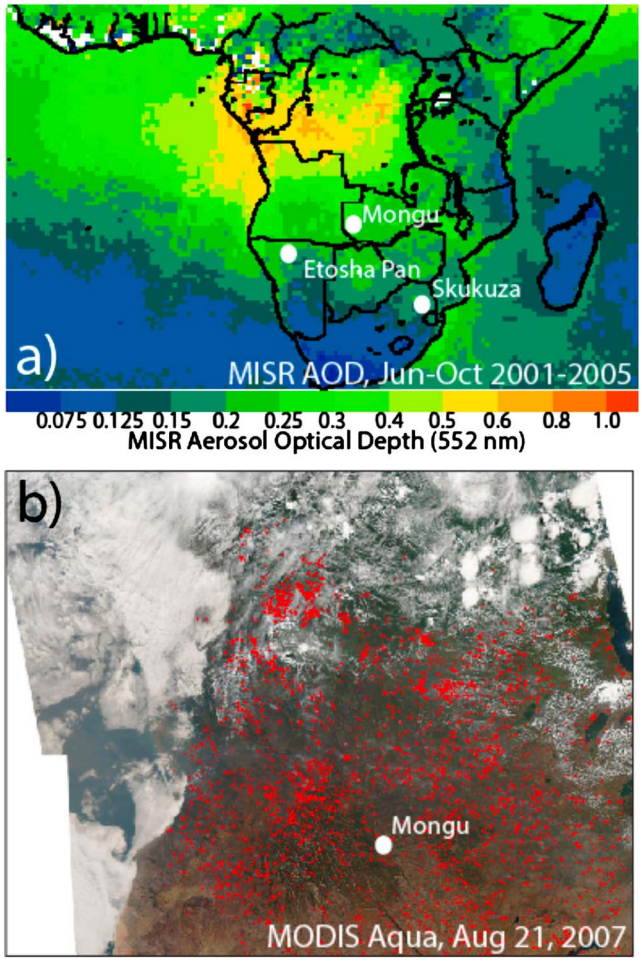

Figure 1. (a) Average midvisible AOD retrieved from MISR for the primary southern Africa burning season months of June to October for the years 2001 to 2005. Also shown are the AERONET sites discussed in this paper located within this biomass-burning region. (b) A single-day MODIS image from 21 August 2007 showing the fire counts in red and the location of the Mongu AERONET site.

through 2009. However, the retrievals of SSA from Mongu were not available from 2005 to 2009 due to problems with either the temperature sensor (needed in order to correct the 1020 nm data) and/or obstructions in the collimator that measures sky radiances. Other AERONET sites which were analyzed in this study were located in Etosha Pan National Park (19°10′S; 15°54′E), Namibia and Skukuza (25°59.5′S; 31°35′E; in Kruger National Park), South Africa. The time period of the analysis, which is July to early November, coincides with the biomass burning associated with agricultural practices and land management and thus the highest levels of AOD from biomass burning [*Scholes et al*., 1996]. Subsidence from anticyclonic circulation is a dominant meteorological feature during much of the biomass-burning season in this region with four stable vertical layers identified in the troposphere [*Garstang et al*., 1996; *Anderson et al*., 1996]. Altitudinal layering of aerosols associated with temperature inversions was observed with a micropulse lidar at a site in South Africa during SAFARI 2000 [*Campbell et al*., 2003]. This atmospheric stability often results in cloudless or nearly cloudless sky conditions for extended periods over land for much of the biomass-burning season.

2.2. AERONET Instrumentation

[9] The Cimel Electronique CE-318 sun-sky radiometer measurements reported in this paper were made with instruments that are a part of the Aerosol Robotic Network (AERONET) global network. These instruments are described in detail in *Holben et al*. [1998]; however, a brief description will be given here. The automatic tracking Sun and sky scanning radiometers made direct Sun measurements with a 1.2° full field of view every 15 min at 340, 380, 440, 500, 675, 870, 940, and 1020 nm (nominal wavelengths). The direct Sun measurements take ~8 s to scan all eight wavelengths, with a motor-driven filter wheel positioning each filter in front of the detector. These solar extinction measurements are then used to compute aerosol optical depth (AOD) at each wavelength except for the 940 nm channel, which is used to retrieve total columnar (or precipitable) water vapor in centimeters. The filters utilized in these instruments were ion-assisted deposition interference filters with band pass (full width at half maximum) of 10 nm, except for the 340 and 380 nm channels at 2 nm band pass. The estimated uncertainty in measured AOD, due primarily to calibration uncertainty, is ~0.010–0.021 for field instruments (which is spectrally dependent with the higher errors in the UV) [*Eck et al*., 1999]. *Schmid et al*. [1999] compared AOD values derived from four different solar radiometers (including an AERONET sun-sky radiometer) operating simultaneously together in a field experiment and found that the AOD values from 380 to 1020 nm agreed to within 0.015 (root-mean-square; RMS), which is similar to our estimated level of uncertainty in AOD measurement for field instruments. The spectral aerosol optical depth data (all data are AERONET version 2 level 2) have been screened for clouds following the methodology of *Smirnov et al*. [2000], which relies on the greater temporal variance of cloud optical depth versus aerosol optical depth. The sky radiances measured by the sun/sky radiometers are calibrated versus the 2 m integrating sphere at the NASA Goddard Space Flight Center, to an absolute accuracy of ~5% or better.

2.3. Inversion Methodology

[10] The Cimel sky radiance measurements in the almucantar geometry (fixed elevation angle equal to solar elevation and a full 360° azimuthal sweep) at 440, 675, 870, and 1020 nm (nominal wavelengths) in conjunction with the direct sun-measured AOD at these same wavelengths were used to retrieve optical equivalent aerosol size distributions and refractive indices. Using this microphysical information, the spectral dependence of SSA is calculated. The algorithm of *Dubovik and King* [2000] with enhancements detailed in *Dubovik et al*. [2006] was utilized in these retrievals, known as Version 2 AERONET retrievals. Level 2 quality-assured retrievals [*Holben et al*., 2006] are presented in this paper. The Version 2 AERONET algorithm determines the percentage of spherical (versus spheroidal shape) particles required to give the best fit to the measured spectral sky radiance angular distribution. Further details on the Version 2 algorithm and the improved specification of

surface bidirectional reflectance can be found in *Dubovik et al*. [2006] and *Eck et al*. [2008].

[11] Almucantar sky radiance measurements were made at optical air masses of 4, 3, 2, and 1.7 in the morning and afternoon, and once per hour in between. In order to ensure sky radiance data over a wide range of scattering angles, only almucantar scans at solar zenith angles (SZA) greater than 50° are analyzed and presented here (the maximum SZA is ~76°). To eliminate cloud contamination from the almucantar directional sky radiance data, we require the radiances to be symmetrical on both sides of the Sun at equal scattering angles [*Holben et al*., 2006]. The stable performance of the inversion algorithm was illustrated in sensitivity studies performed by *Dubovik et al*. [2000] where the perturbations of the inversion resulting from random errors, possible instrument offsets, and known uncertainties in the atmospheric radiation model were analyzed. Their work employed retrieval tests using known size distributions to demonstrate successful retrievals of mode radii and the relative magnitude of modes for various types of bimodal size distributions such as those dominated by a submicron accumulation mode or distributions dominated by supermicron coarse mode aerosols. To ensure sufficient sensitivity to aerosol absorption, only almucantar scans where AOD (440 nm) > 0.4 [*Dubovik et al*., 2000] were analyzed for the investigation of the characteristics of spectral refractive indices and single scattering albedo. Although very few direct comparisons of size distribution between in situ and AERONET retrievals have been made, there are several aerosol types in specific regions that have been or can be compared. For example, *Reid et al*. [2005a] present a table where the volume median radius of smoke from various major biomass-burning regions (South America, southern Africa, North America (boreal, temperate)) are compared. For all three of these regions, the volume median diameters of the in situ versus the AERONET retrievals are often within ~0.01 μm of each other. Additionally, for fine-mode biomass-burning aerosols in southern Africa (including Zambia), *Leahy et al*. [2007] found a mean discrepancy in 550 nm SSA between in situ measurements and AERONET retrievals of −0.01 for five coincident flights over AERONET sites, thus indicating excellent agreement.

2.4. MODIS and MISR Satellite Retrievals of AOD

[12] In this study, we examine the potential for SSA induced bias in satellite AOD retrievals from three primary datasets. First, the over land MODIS data C5 products of *Levy et al*. [2007a] which were co-located with AERONET AOD data at the Mongu site within ±30 min of overpass. These retrievals vary in size from 10×10 km at nadir, to ~40×20 km at the swath edge. *Hyer et al*. [2011] compared MODIS retrieved AOD to AERONET retrievals from the Mongu site for 2005–2008 and found r^2 of 0.61/0.56 and slope biases of 0.83/0.88 for Terra and Aqua MODIS, respectively. In general for southern Africa, *Hyer et al*. [2011] found that prognostic RMS errors were on the order of the greater of 0.06 or $0.00 + 0.28\ \mathrm{AOD}_T$ for Terra and 0.07 or $-0.02 + 0.39 * \mathrm{AOD}_A$ for Aqua where the AOD is taken as the retrieved AOD. Much of this RMS error can be attributed to the slope biases. In the current paper, we also examined MISR v22 retrievals [*Diner et al*., 2010] in like manner to the operational MODIS C5. Retrieval size is 21×21 km throughout the swath. *Kahn et al*. [2010] examined MISR performance at the Mongu site, finding excellent correlation ($r^2 = 0.9$) but a slight low bias (slope of 0.84). To our knowledge, no RMS errors have been formulated for the site, outside of what we will present later in this paper. Intercomparison of MODIS and MISR data by *Shi et al*. [2011] showed reasonable regression coefficients for collocated retrievals (r^2 range from 0.7 to 0.85) but with MODIS having 20% higher values in slope. This result is somewhat at odds with AERONET-based comparisons.

[13] In addition to the standard operational MODIS and MISR products, we also examined the level 3 operational data assimilation grade MODIS product [*Hyer et al*., 2011] used by the US Navy [*Zhang et al*., 2008]. In this product, data are screened for a number of known artifacts, regression corrections are made for region-wide biases, and a final 1×1° aggregated product is generated. Estimated prognostic RMS errors for this product are the greater of 0.05 or $0.03 + 0.19\ \mathrm{AOD}_T$ for Terra and 0.05 or $-0.01 + 0.21 * \mathrm{AOD}_A$. Much of this improvement is due to the implementation of a regional slope correction.

2.5. OMI Satellite Retrievals of SSA

[14] The Ozone Monitoring Instrument (OMI) on the Aqua satellite is a high-resolution spectrograph in operation since September 2004 [*Levelt et al*., 2006]. OMI observations at 354 nm and 388 nm are used in an inversion algorithm (OMAERUV) to retrieve aerosol single scattering albedo [*Torres et al*., 2007]. The physical basis for detecting and quantifying aerosol absorption in the near UV is the interaction between molecular scattering and particle absorption that generates a unique signal clearly associated with aerosol absorption [*Torres et al*., 1998]. This radiative transfer interaction is the basis of the Absorbing Aerosol Index, a qualitative indicator of aerosol absorption, developed originally from TOMS observations [*Hsu et al*., 1996; *Herman et al*., 1997], and produced routinely since then from observations by sensors with near-UV observing capability. Quantitative information on aerosol absorption can be derived by an inversion procedure. The OMAERUV retrieval technique uses precalculated radiances at 354 and 388 nm to simultaneously retrieve both aerosol optical depth and single scattering albedo. A priori information on particle size distribution and aerosol layer height is required. Retrieval algorithm details are given in *Torres et al*. [2007], and recent upgrades are discussed by *Jethva and Torres* [2011] and *Torres et al*. [2012].

3. Results

3.1. Seasonal Variation of Aerosol Absorption—AERONET Data

[15] Multiyear measurements made by the Cimel sun-sky radiometer at the AERONET site in Mongu, Zambia provide the most complete data set to investigate the seasonality of aerosol optical depth and absorption in the southern Africa biomass-burning region. In Figure 2, we present the monthly averages of Level 2 direct sun-measured 500 nm AOD at Mongu from measurements made from 1995 to 2009, similar to that shown in *Queface et al*. [2011]. Monthly means were computed from daily means, with a minimum of 9 days per month used as a threshold for good sampling, resulting in

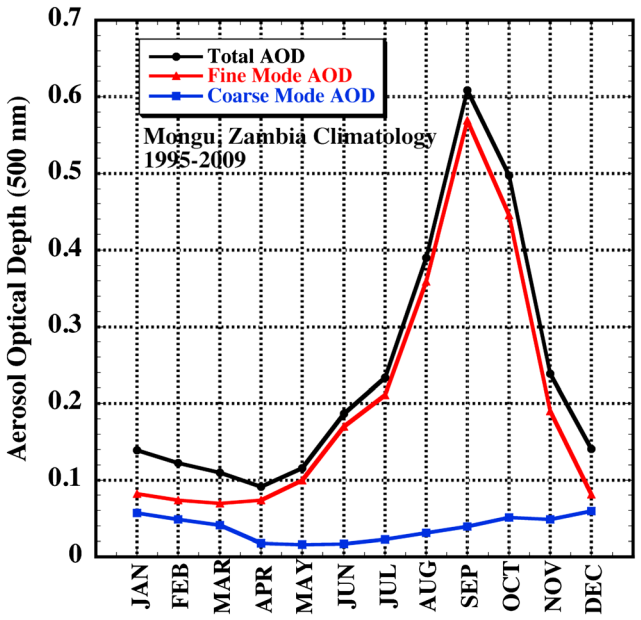

Figure 2. Monthly mean AOD at 500 nm at the Mongu, Zambia AERONET site from 1995 to 2009. A threshold of 9 days minimum per month was required to ensure adequate sampling, resulting in 8 to 13 years of data being averaged for each month. The fine- and coarse-mode AODs were computed using the Spectral Deconvolution Algorithm (SDA).

8 to 13 years of data being averaged for each month. The biomass-burning season in Mongu begins in June with elevated AOD and ends in November. Also shown in Figure 2 are the fine- and coarse-mode AOD values that are computed from the Spectral Deconvolution Algorithm (SDA) described in *O'Neill et al*. [2001, 2003] based on the measured AOD spectra from 380 to 870 nm and the assumption of a bimodal size distribution. The SDA retrievals of fine mode fraction (FMF) of AOD at 500 nm are ~0.03 to 0.05 lower on average than almucantar-retrieved FMF [*Eck et al*., 2010], likely due in part to the small-sized particle "wing" of the coarse mode attributed to coarse-mode AOD in the SDA, while this wing is included in the fine mode of the Dubovik algorithm since a particle radius cutoff is selected to define the two modes [*O'Neill et al*., 2003]. Another possible reason for the bias could be that the SDA retrieval does not explicitly account for effects of variation in the refractive index, which is a source of SDA retrieval error. It can be seen in Figure 2 that fine-mode aerosol particles dominate the total AOD during the biomass-burning season, while coarse-mode AOD is elevated in the rainy season, likely due to some cloud contamination in those months [*Eck et al*., 2003].

[16] The data shown in Figure 3 are daily averages of single scattering albedo for years with significant numbers of almucantar retrievals at the Mongu site, 1997 to 2005, excluding 2000. The year 2000 data were excluded due to a problem with the sky radiance calibration for that instrument in that year [*Eck et al*., 2003]. The SSA retrievals at 440 nm are shown only for observations where AOD at 440 nm exceeded 0.4, thus ensuring sufficient aerosol loading to limit SSA uncertainty at ~0.03 or less. In Figure 3a, data are shown from May to November, and it is noted that from late May to early June, the SSA values show a relatively large degree of variability with some higher values than measured in July. The reason for this large variability in the May–June preseason is not well known. It may possibly be caused in part by smoke from burning to the north of Zambia, some of which is more densely forested. Clearly, the majority of the data with moderate to high AOD occur from July to October plus a few in November (a total of 300 days of data), as this is the primary biomass-burning season in the region that is predominantly savanna and woodland [*Cooke et al*., 1996]. Therefore, we will focus on this time period for further analysis of the Mongu data. Figure 3b shows the daily average SSA data time series for the months of July–November, and there is clearly a linear trend of increasing SSA as the burning season progresses, with a linear fit explaining 49% of the variance. It is noted that we found no trend of SSA as a function of AOD magnitude ($r^2 = 0.02$). What we did

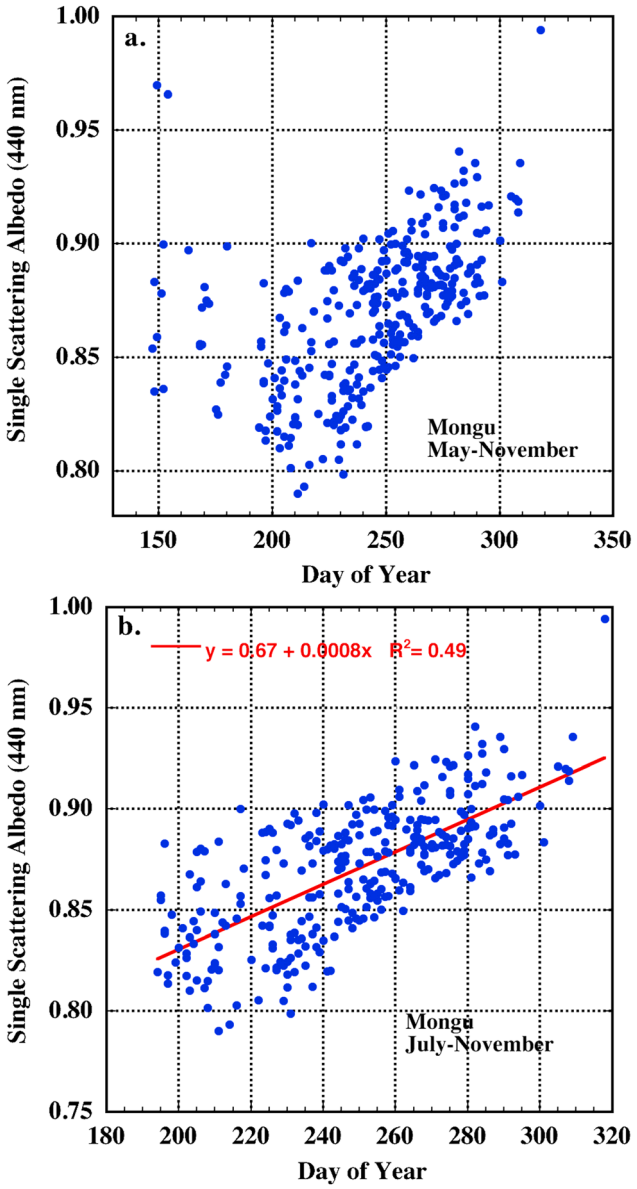

Figure 3. Time series of single scattering albedo (440 nm) at Mongu, Zambia for cases where AOD (440 nm) > 0.4 from (a) May to November and from (b) July to November, the main biomass-burning season.

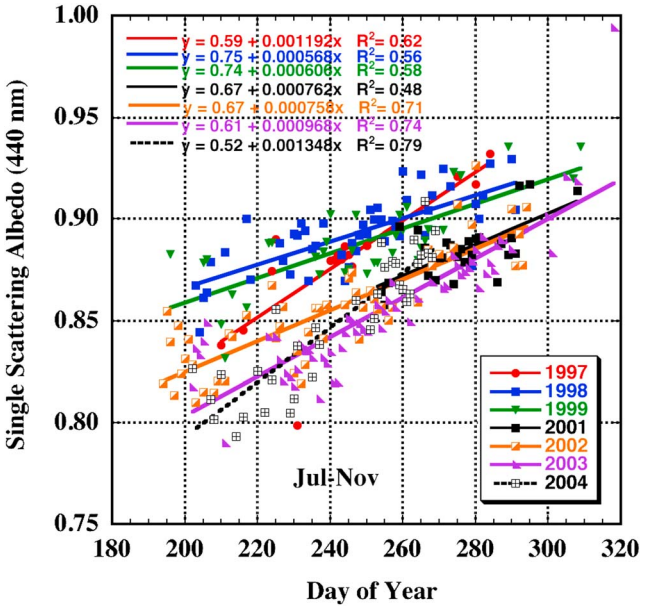

Figure 4. Similar to Figure 3b, the burning season time series of SSA (440 nm) for Mongu, but with linear regression analysis made on each year separately.

find, however, was that there is an interannual shift in the overall SSA magnitude. This is demonstrated in Figure 4 where the data for the individual years are analyzed separately. It is hence noted that part of the scatter in Figure 3 is due to variation in SSA magnitudes between years, with higher values in 1997–1999. The data for all 7 years however show a similar increase in SSA through the entire burning season with linear regression fits explaining from 48% to 79% of the variance in individual years. The year 2005 was excluded in this figure since nearly all data from August and September 2005 were missing due to logistical problems. The reason for the higher SSA values in 1997–1999 is unknown, but may possibly be due to interannual differences in biomass fuel types (woody versus grasses) burned in different proportions, but may also be due to biases in the Cimel sky radiance calibrations from year to year. The accuracy of the direct sun AOD measurement is highly accurate (~0.01 in visible and near infrared) [*Eck et al.*, 1999] but the sky radiance calibration uncertainty is larger at less than 5% [*Holben et al.* 1998]. The magnitude of the sky radiances will directly affect the retrievals of SSA; therefore, the early year data may possibly be biased high due only to calibration uncertainty. However, regardless of this interannual variability, the data from all individual years show a similar strongly increasing SSA, meaning increasingly weaker absorption, from the beginning to the end of the burning season.

[17] The monthly mean spectral variation of SSA from 440 nm to 1020 nm (all four of the retrieved wavelengths) from the same days as shown in Figure 3b is shown in Figure 5 averaged by month. Although the mean AOD and fine-mode AOD in November are similar to the July monthly mean [*Eck et al.*, 2003; *Queface et al.*, 2011], only six good retrievals of SSA were available in November in all these years of monitoring; this is due to the rapid increase in cloud cover accompanying the start of the rainy season (the dry season months of April–October contribute <10% of the annual mean rainfall amount). A direct sun measurement of AOD can be made in a gap between clouds while the SSA retrieval requires a mostly cloud-free sky radiance scan over a full azimuthal sweep at constant elevation angle equal to the sun elevation (from 15° to 40° elevation angle for a Level 2 almucantar scan). While significant smoke is present in November, the sparseness of the SSA data for this month results in this analysis being more uncertain. We will therefore concentrate on the months of July to October in the following discussion of Figure 5. The SSA at 440 nm in October is 0.058 higher than in July, and the October–July mean SSA differences for 675, 870, and 1020 nm are 0.076, 0.086, and 0.091, respectively. These are large seasonal changes in SSA that may have significant impacts on the retrieval of AOD from satellite using algorithms that require a priori assumption of SSA [*Ichoku et al.*, 2003], and also result in significant changes in aerosol direct and semidirect radiative forcings. It is noted that the climatological average SSA values for African savanna in Zambia (mostly data from Mongu) given by *Dubovik et al.* [2002] from pre-Version 1 AERONET data are within 0.01 or less at all wavelengths of the September monthly mean shown in Figure 4. The updated Version 2 database SSA climatology given by *Giles et al.* [2012] for Mongu (based on the entire season) is also within 0.01 of the September average shown in Figure 5, except for 1020 nm which is 0.02 higher than *Giles et al.* (2012). This similarity in climatological biomass-burning season average to the September monthly mean occurs since September has the most retrievals of any month and since lower SSA values are retrieved in July and August and higher SSA in October and November.

[18] The spectral variation of SSA can further be characterized by the variation in the aerosol absorption Ångström exponent. The absorption Ångström exponent (AAE) is computed from spectral absorption optical depths (AAODs)

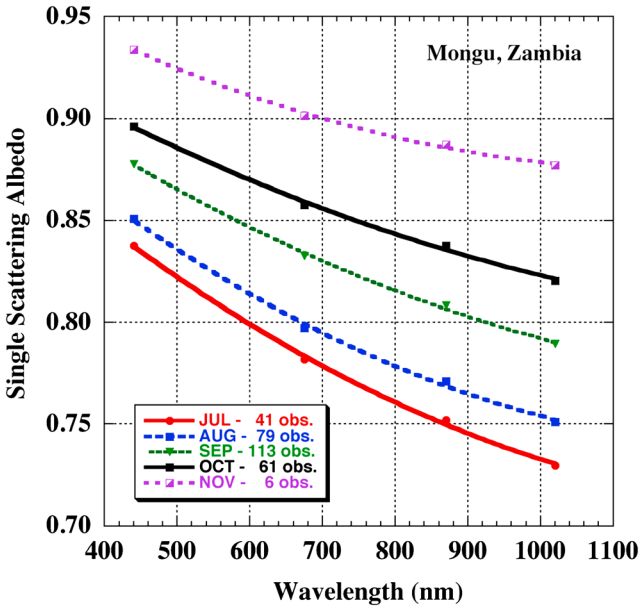

Figure 5. Monthly mean values of spectral SSA for Mongu Zambia from 1997 to 2005 for the burning season months, for all four retrievals wavelengths (440, 675, 870, and 1020 nm).

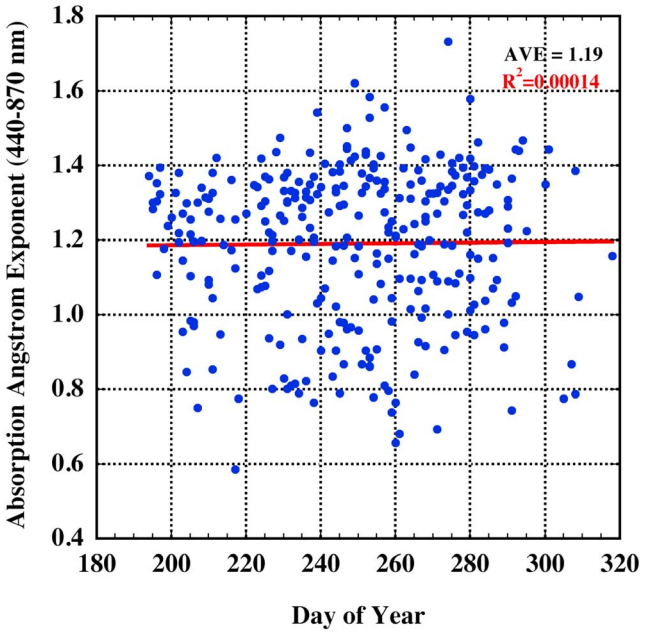

Figure 6. The time series of daily average absorption Ångström exponents (440–870 nm) for the biomass-burning season at Mongu Zambia, showing a lack of any seasonal trend.

which are in turn computed from spectral total extinction AOD and SSA by

$$\mathrm{AAOD} = \mathrm{AOD}\,(1 - \mathrm{SSA}) \tag{1}$$

[19] The negative of the mean fitted slope of the AAOD with wavelength in logarithmic coordinates defines the AAE. Daily mean values of AAE for Mongu from July to November are shown in Figure 6 for the same years as shown in Figure 3. The majority of the daily mean values of AAE ranged from ~0.80 to 1.5 with an overall biomass-burning season mean of 1.19. Theoretically, fine-mode aerosol with absorption determined exclusively by black carbon (BC) would have AAE equal to 1.0, since BC is expected to have a spectrally constant imaginary refractive index (k) [*Bergstrom et al*., 2002; *Bergstrom et al*., 2007]. In fact, the retrievals of imaginary refractive index (k) for this Mongu data do show relatively small wavelength dependence, as seen in the spectral monthly means in Figure 7. Therefore, this seasonal mean value of AAE of ~1.20 at Mongu and small spectral variation of imaginary refractive index both suggest that BC is the dominant absorber in the visible and near-infrared wavelengths for this biomass-burning aerosol, which is consistent with in situ measurements [*Ward et al*., 1996; *Reid and Hobbs*, 1998]. There is also a lack of any seasonal trend in daily average AAE at Mongu (Figure 6; $r^2 = 0.0001$), therefore implying that BC is the dominant absorbing aerosol component throughout the entire biomass-burning season. For smoke produced by combustion of various biomass fuels, measured in situ under controlled laboratory conditions, *Lewis et al*. [2008] found AAE as high as 2.5 (532 to 870 nm) at high SSA (near unity) while AAE values approached 1.0 for SSA < 0.8 at 532 nm. The measured organic carbon to total carbon ratio was highest for the smoke with the highest AAE and SSA and lowest for the lowest SSA values measured.

[20] To further investigate the reasons for the trend in aerosol single scattering albedo throughout the biomass-burning season, we examine data on both the retrieved aerosol size and the complex refractive indices. In Figure 8a we show the daily averages of Ångström exponent (440–870 nm) computed using direct sun-measured AOD at 440, 500, 675, and 870 nm from linear regression, for July to November (associated with the retrieval dates and times in Figure 3b). The Ångström exponent computed from a wide wavelength range has been shown to be a general indicator of particle size and fine/coarse-mode fraction [*Eck et al*., 1999; *Eck et al*., 2010]. The values of $\alpha_{440-870}$ range primarily from ~1.7 to ~2.0 with a mean of 1.85 which is typical of fine-mode (submicron radius) dominated aerosol from biomass-burning regions [*Holben et al*., 2001; *Eck et al*. 2003; *Schafer et al*., 2008]. Additionally, the lack of any seasonal trend ($r^2 = 0.02$) in $\alpha_{440-870}$ suggests that the particle size and fine-mode fraction did not change significantly from July to November. The short wavelength range Ångström exponent (380–500 nm) is much more sensitive to variation in fine-mode particle size [*Reid et al*., 1999; *Eck et al*., 2001], and this also exhibited no significant seasonal trend ($r^2 = 0.06$; mean = 1.52; not shown). It is noted that the SDA fine-coarse mode AOD shown in Figure 2 would suggest a decrease in Ångström exponent at the end of the burning season in October and especially in November, as compared to the lack of trend shown in Figure 8a. However, the data shown in Figure 8a are only from observations associated with Level 2 almucantar retrievals that have the additional more rigorous application of cloud screening of sky radiance data symmetry and effective sky radiance noise filtering. The result is only 6 days of data with Level 2 almucantars from November in the entire Mongu data set (see Figure 5 legend), while there are 223 days with level 2

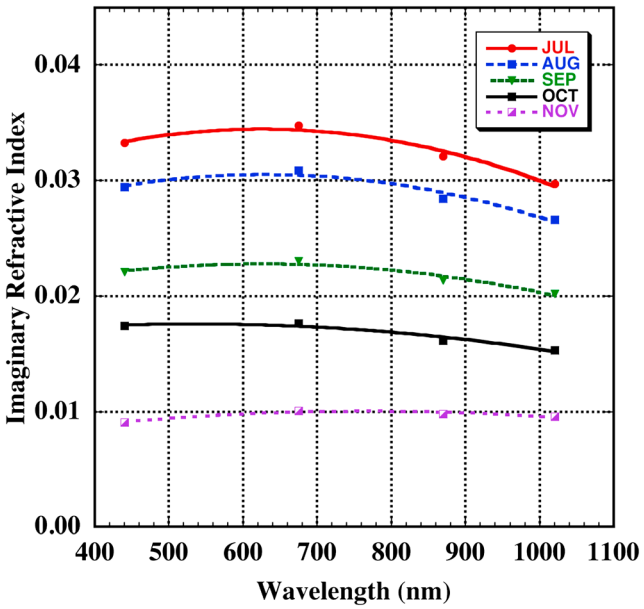

Figure 7. Monthly mean spectral imaginary refractive indices (similar to SSA in Figure 4) for the biomass-burning season months in Mongu, Zambia.

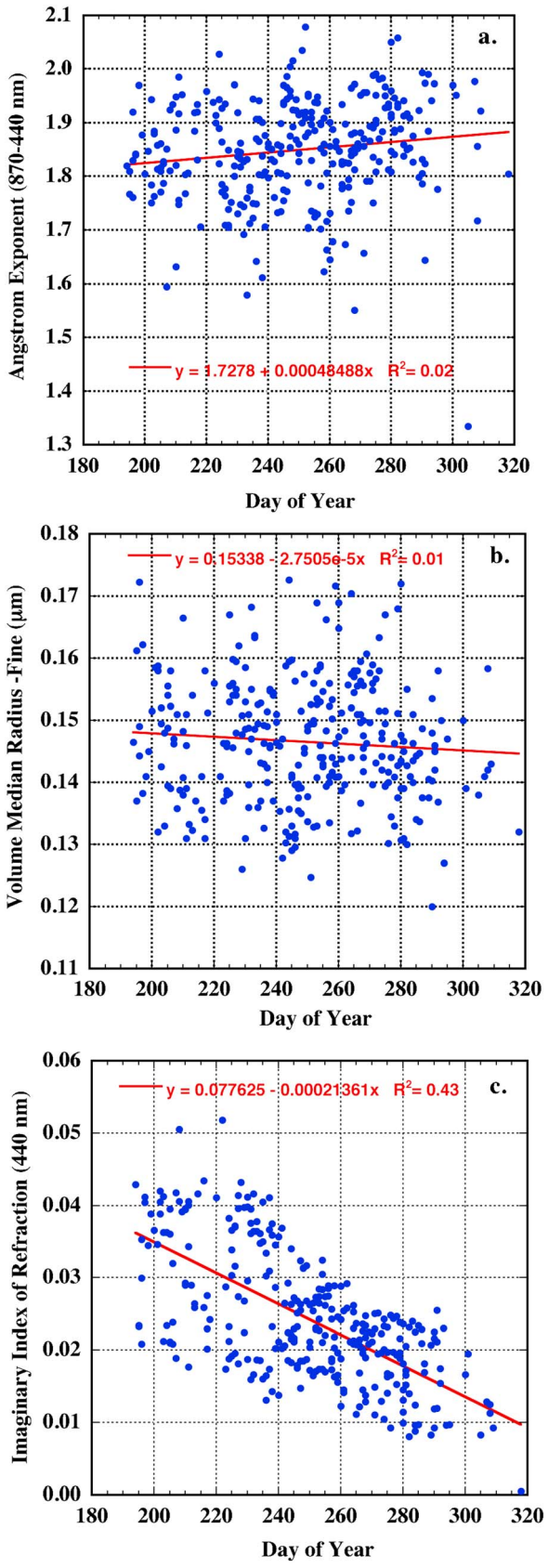

Figure 8. Time series at Mongu, Zambia during the biomass-burning season of daily means of (a) Ångström exponent (440–870 nm), (b) fine mode volume median radius (µm), and (c) 440 nm imaginary index of refraction.

direct sun AOD data shown in Figure 2, which include some days with partial cloud contamination.

[21] Prior studies have analyzed the AERONET volume size distribution retrievals in Mongu and other sites in Zambia [*Eck et al.*, 2001; *Dubovik et al.*, 2002; *Eck et al.*, 2003]. As previously mentioned, the mean volume radius for biomass-burning aerosols in this region from AERONET has compared well with in situ measurements, within ~0.005 µm radius [*Reid et al.*, 2005a]. In Figure 8b, the time series of fine-mode volume median radius from the AERONET retrievals shows most data within ~0.13 to 0.16 µm radius (mean = 0.146 µm), and with no seasonal trend ($r^2 = 0.01$), which is consistent with the lack of trend in Ångström exponent. Since aerosol size showed no trend throughout the burning season, this suggests that aerosol growth through aging, coagulation, or hygroscopic swelling (at higher relative humidity) can be ruled out as a significant underlying reason for the seasonal trend in single scattering albedo. The seasonal trend of the asymmetry parameter was also analyzed, and the percentage of variance explained by linear regression ranged from less than 0.1% to 1.5% from 440 nm to 870 nm. Therefore there was no significant observed trend in the AERONET retrievals of the aerosol scattering phase function throughout the biomass-burning season. The retrieved real part of the refractive index also shows no significant seasonal variation ($r^2 = 0.06$) and has a seasonal mean ranging from 1.49 at 440 nm to 1.51 at 1020 nm, therefore has little influence on the SSA trend. On the other hand, the imaginary index of refraction (Figure 8c), which accounts for absorption, does exhibit a significant downward seasonal trend. In fact, the linear regression fit explains 43% of the variance, very similar to the 49% of the variance explained by the SSA versus day of year linear fit seen in Figure 3b. Since we had previously suggested from analysis of the AAE that black carbon is likely the primary absorbing aerosol component at Mongu, then the downward trend in k suggests that the black carbon content in the aerosol is decreasing as the burning season progresses and is also the primary reason for the seasonal trend in SSA.

[22] In order to investigate whether this trend in SSA is a local phenomenon, we analyzed the data from the Etosha Pan, Namibia site which is ~885 km to the southwest of Mongu. The AERONET data from the Etosha Pan site were only available for one burning season, August to November 2000 for the SAFARI 2000 campaign. Hence, we analyzed individual almucantar retrievals versus day of year, rather than daily averages of the retrievals as was done previously for Mongu. Figure 9a shows the temporal trend of SSA, which is very similar to the trend observed at Mongu, in fact within less than 0.01 of the trends observed at Mongu for the years 2001 to 2004 (Figure 4) and with a similar r^2 value (0.69) from linear regression. The trend of decreasing imaginary refractive index as the burning season progresses (Figure 8b) at Etosha Pan is also very similar to the trend observed at Mongu, and the 69% of variance explained by the linear fit is the same as for the SSA trend at Etosha Pan. Similar to Mongu, there was no significant trend in aerosol size with Ångström exponent (440–870 nm) varying from ~1.5 to 2.1 indicating all fine mode dominated smoke, except for the two last points at day 318 that was a dust event with $\alpha_{440-870} < 0.15$. Therefore, the similarity of the SSA and

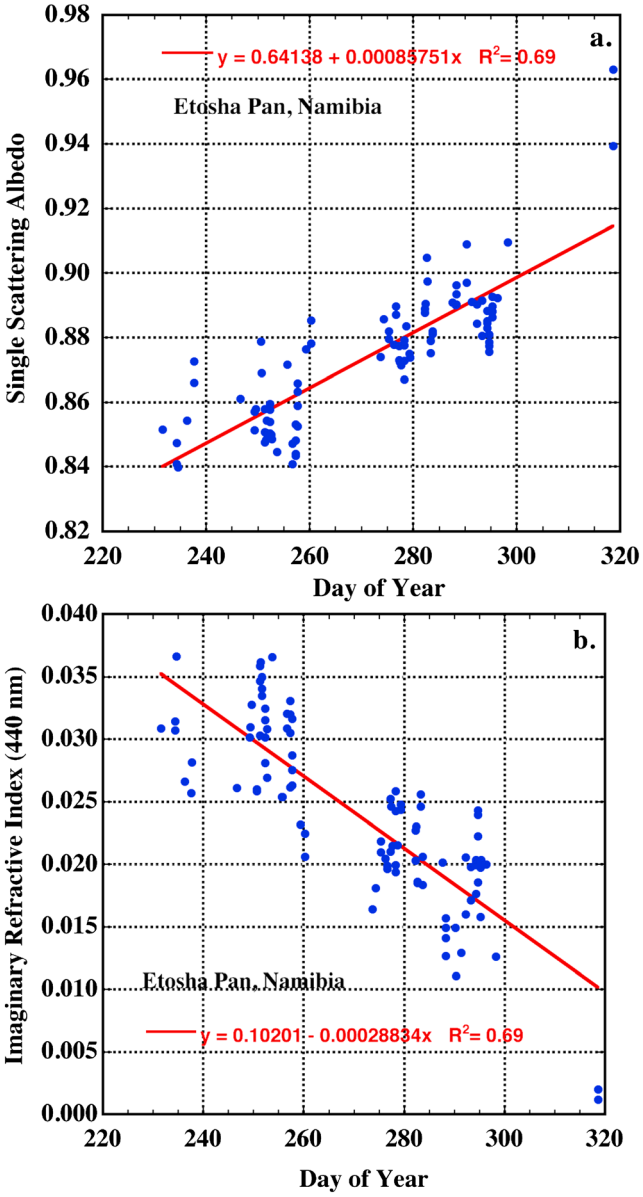

Figure 9. Biomass-burning season time series of individual retrievals at Etosha Pan, Namibia, for (a) single scattering albedo at 440 nm and (b) imaginary refractive index at 440 nm.

imaginary index trends at both Etosha Pan and Mongu suggests that this burning season trend in aerosol absorption is coherent over a relatively large region.

[23] The Skukuza, South Africa site is further yet from Mongu and in another direction, ~1395 km to the southeast. The SSA at 440 nm is plotted versus day of the year for this site in Figure 10. The seasonal trend in SSA at Skukuza shows mainly lower values in the primary biomass-burning season of July–October with large variation however versus higher values in other months. A significantly less coherent trend is seen throughout the burning season however than was observed at either the Mongu or Etosha Pan sites. There is no trend in Ångström exponent (440–870 nm) for the July–December interval ($r^2 = 0.00$; mean $\alpha_{440-870} = 1.66$), and while there is a downward trend in imaginary refractive index, it shows more scatter ($r^2 = 0.10$) than the trend in SSA ($r^2 = 0.16$) over the July–December interval. This variability may largely be due to mixtures of other aerosol types besides those from open biomass burning in this region. *Piketh et al.* [1999] analyzed in situ ground-based measurements at several sites in South Africa (including one very near Skukuza) and concluded that sulfate aerosol from industrial fossil fuel combustion and mineral dust was the main aerosol types in the region. Since sulfate is fine-mode nonabsorbing aerosol, the relatively high SSA values (and $\alpha_{440-870}$ predominately higher than 1.40) retrieved by AERONET for the total atmospheric column at Skukuza were very likely the result of aerosol mixtures with a significant sulfate component.

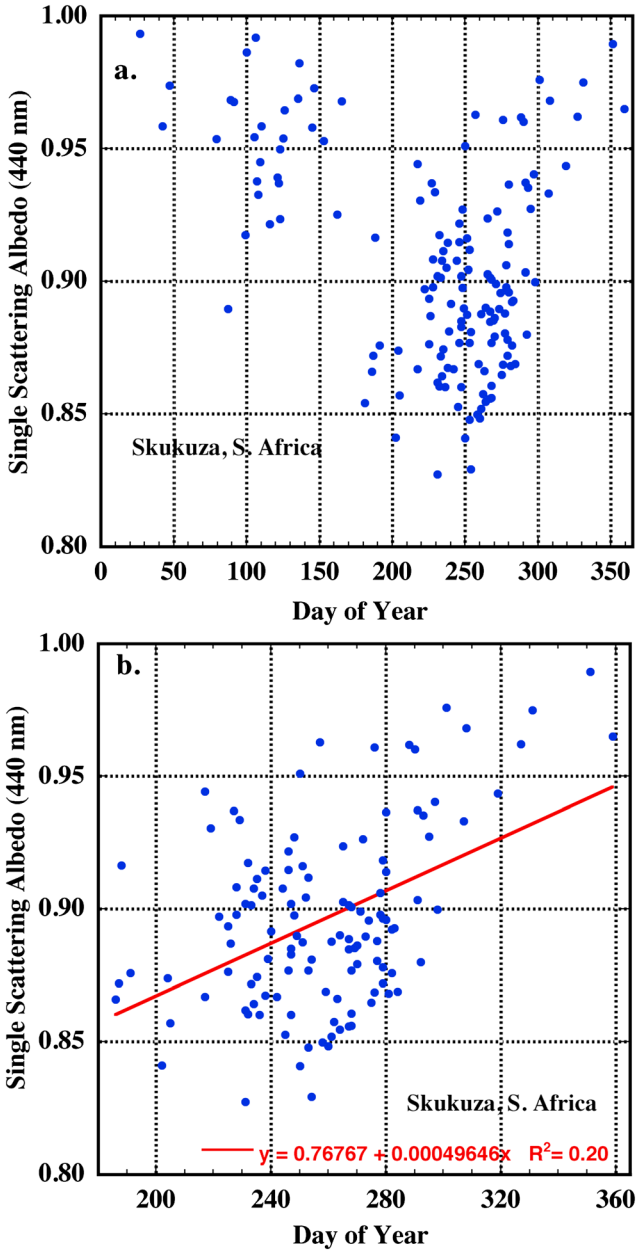

Figure 10. Time series of the SSA (440 nm) at Skukuza, South Africa, for (a) the entire year and (b) the biomass-burning season of July to December.

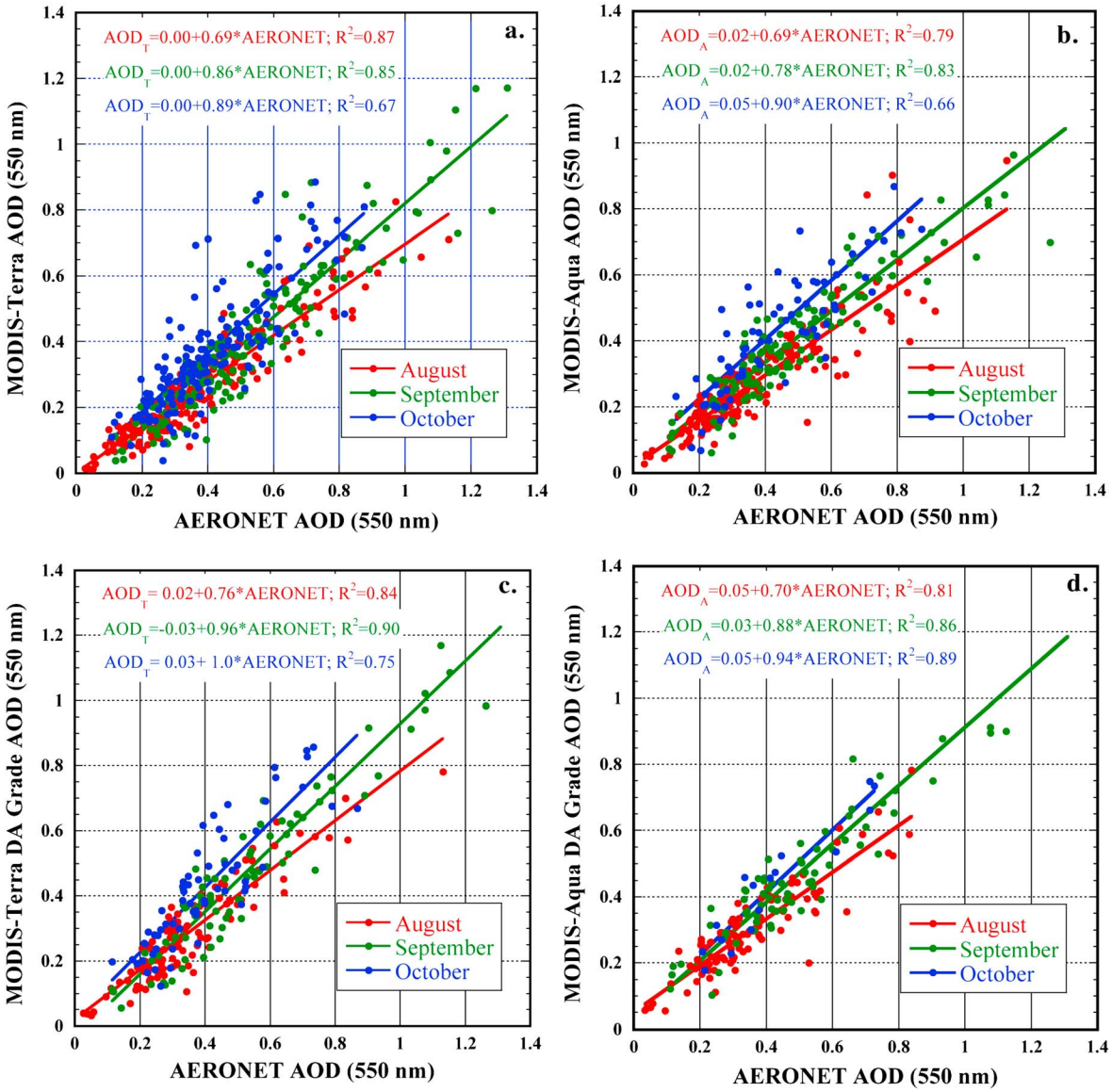

Figure 11. Comparison of MODIS retrievals (dark target algorithm) from both (a) Terra 2001–2010 and (b) Aqua 2003–2010 of AOD at 550 nm to AERONET measurements at Mongu, Zambia, with data separated for the primary burning season months of August, September, and October. Figures 11c and 11d are the same as Figures 11a and 11b but for the NRL data assimilation grade MODIS product of *Hyer et al.* [2011].

3.2. Seasonal Analysis of MODIS and MISR AOD Retrievals

[24] Any consistent seasonal shift in SSA has the potential to impact satellite AOD retrievals and thus result in a seasonally varying bias which could be perceived as random noise in a large verification study. Retrieval of AOD from the standard MODIS algorithms, for example, is dependent on the a priori assumption of a value of aerosol absorption [*Remer et al.*, 2005; *Levy et al.*, 2007a, 2007b]. Deviation from the assumed values has a compounding effect on retrieval bias as AODs increase into multiple scattering environments. AERONET measured AOD is highly accurate (~0.01 in the visible and near infrared) and therefore comparison to satellite retrievals allows for analysis of the likely reasons for potential biases, primarily either from errors in characterizing surface reflectance or in allowing for a realistic enough aerosol model. Given the high AODs found in the southern Africa smoke plume, the seasonal variation in AERONET inverted SSA provides a natural laboratory to test the impact of SSA on satellite AOD retrieval error. Indeed, as we found no systematic seasonal microphysical changes in the retrievals other than absorption, the Mongu site allows the examination of a rarely occurring "partial derivative" of satellite retrieval microphysical models.

[25] To begin, comparisons of AOD retrievals from both Terra and Aqua satellite MODIS sensors against the Mongu AERONET site are presented in Figures 11a and 11b, respectively. Comparisons of AOD are shown for 550 nm with the AERONET data being interpolated to 550 nm. This matchup was described in section 2. To observe the influence of seasonal variation of SSA, data are divided into the three core months of burning, August, September, and October,

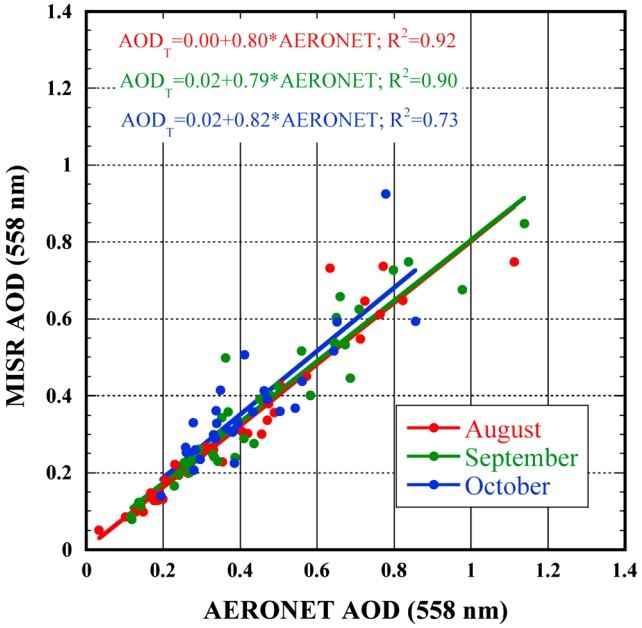

Figure 12. Similar to Figure 11a, but for a comparison of AERONET to MISR retrievals of AOD at 558 nm from data acquired from 2001 to 2009.

utilizing data from 2001 to 2010 for Terra and 2003 to 2010 for Aqua. Taken as a bulk regression, the comparison of MODIS to AERONET for all data yields values of MODIS that equals $-0.01 + 0.82 * \text{AERONET}$ $r^2 = 0.78$ and $0.02 + 0.78 * \text{AERONET}$ $r^2 = 0.76$ for Terra and Aqua, respectively. Thus, correlation is quite good but there appears to be a persistent 20% low bias in the slope. However, from Figure 11a where we perform regressions by month, it is seen that the bulk MODIS comparison is made from a progression of biased but generally even higher correlated populations where the slope increases in time. For example, for MODIS Terra, slopes progress from 0.69 to 0.86 to 0.89, for August, September, and October, respectively. This corresponds to an increase in SSA of about 0.05 over this period. Because regressions can be misleading, it is perhaps even more illustrative to perform a simple average of data points in the middle of the population, say for MODIS, AODs between 0.45 and 0.55. From the data shown in Figure 11a, if Terra MODIS reports an AOD of 0.5, the real AOD is likely 0.71, 0.61, and 0.60 for August, September, and October, respectively. Hence, from both an AOD and particle/mass burden point of view, the reported value is likely only 70%, 82%, and 83% of the true value, respectively, for these months.

[26] While the above comparison is suggestive of SSA-induced bias in the MODIS C5 retrieval, it is by no means definitive as there are other possible variables with seasonal progression which may have a similar effect. To reduce the effects of additional variables that may contribute to trends, such as lower boundary condition, viewing/sun geometry or persistent cloud artifact, this analysis was repeated using the Naval Research Laboratory (NRL) data assimilation grade product of *Hyer et al.* [2011]. In this case, corrections are made to the MODIS product based on the seasonally increasing surface albedo as well as the progression of sun/view geometry. It should be emphasized, however, that this is an aggregated 1° latitude-longitude resolution product and does not necessarily correspond one to one with the Level 2 analysis above. One particular filter is the requirement of homogeneity on the scene, which by nature excludes not only potential cloud artifacts but also observations of dense plumes near smoke sources. Monthly regression for data assimilation (DA) grade MODIS Terra and Aqua is given in Figures 11c and 11d, respectively. Overall, the DA grade performed overall better in both slope and correlation than the corresponding standard operational runs, yet a seasonal progression in slope is still present. Here, when MODIS DA grade reports an AOD = 0.5, this value is low by 0.07, 0.05, and 0.03 for August, September, and October, respectively, or 87%, 91%, and 98% of the true value for the 3 months. Put another way, the size of the regional correction in MODIS data implemented by *Hyer et al.*, [2011] is of the same magnitude as the seasonal variation in the operational product.

[27] Finally, we performed a data comparison with MISR. The MISR retrieval has an advantage over retrievals that utilize static assumptions in that its multiple look angles allow for a more robust treatment of aerosol particle absorption and the surface reflectance. Figure 12 provides a scatterplot similar to Figure 11a, where MISR AOD is plotted against the Mongu AERONET site by month for 2001 to 2009. Because MISR has a narrow swath, it has perhaps only four opportunities per month to observe the Mongu site and consequently many fewer data points than provided by MODIS. Here we find a much more consistent retrieval by month, with no consistent seasonal dependency in retrieval bias, although a persistent slope of ~0.8 exists. For the entire data set, a MISR retrieved AOD when average AOD = 0.5 is low biased by 0.08, or 86% of the true value. Clearly, MISR does not appear to be impacted by variability in the biomass-burning particles SSA.

3.3. Seasonal Variation of Aerosol Absorption—OMI Satellite Retrievals

[28] Using OMI data, we may be able to assess the spatial extent of the southern Africa region which may be experiencing a seasonal trend in SSA. The OMI algorithm estimates of SSA at 388 nm [*Torres et al.*, 2007; *Jethva and Torres*, 2011] and the seasonal trend at the Mongu site inferred from OMI data for the years 2005 to 2010 are shown in Figure 13b. Similar to the AERONET retrievals at Mongu (Figure 3b), OMI retrieves a clear trend of increasing SSA as the burning season progresses, although with much more scatter in the satellite-derived estimates. The increase in SSA during the primary days of the burning season, from days 200 to 300, was ~0.06 from OMI versus ~0.08 increase from AERONET. This is a similar magnitude of upward trend, although the AERONET retrievals of SSA are for 440 nm (shortest wavelength), while the OMI retrievals are made for 388 nm. The magnitude of the differences in SSA with wavelength between 388 nm and 440 nm in this region is unknown and a topic of future research. Similar investigation of trend analysis of OMI retrieved SSA was conducted for four additional sites in southern Africa (Figures 13c–13f). Site 1 is located in Angola near the Atlantic coast and inland from the region of persistent stratocumulus cloud cover. Sites 2 and 3 are located to the northeast and east-northeast of Mongu in regions of the Democratic Republic of the Congo and

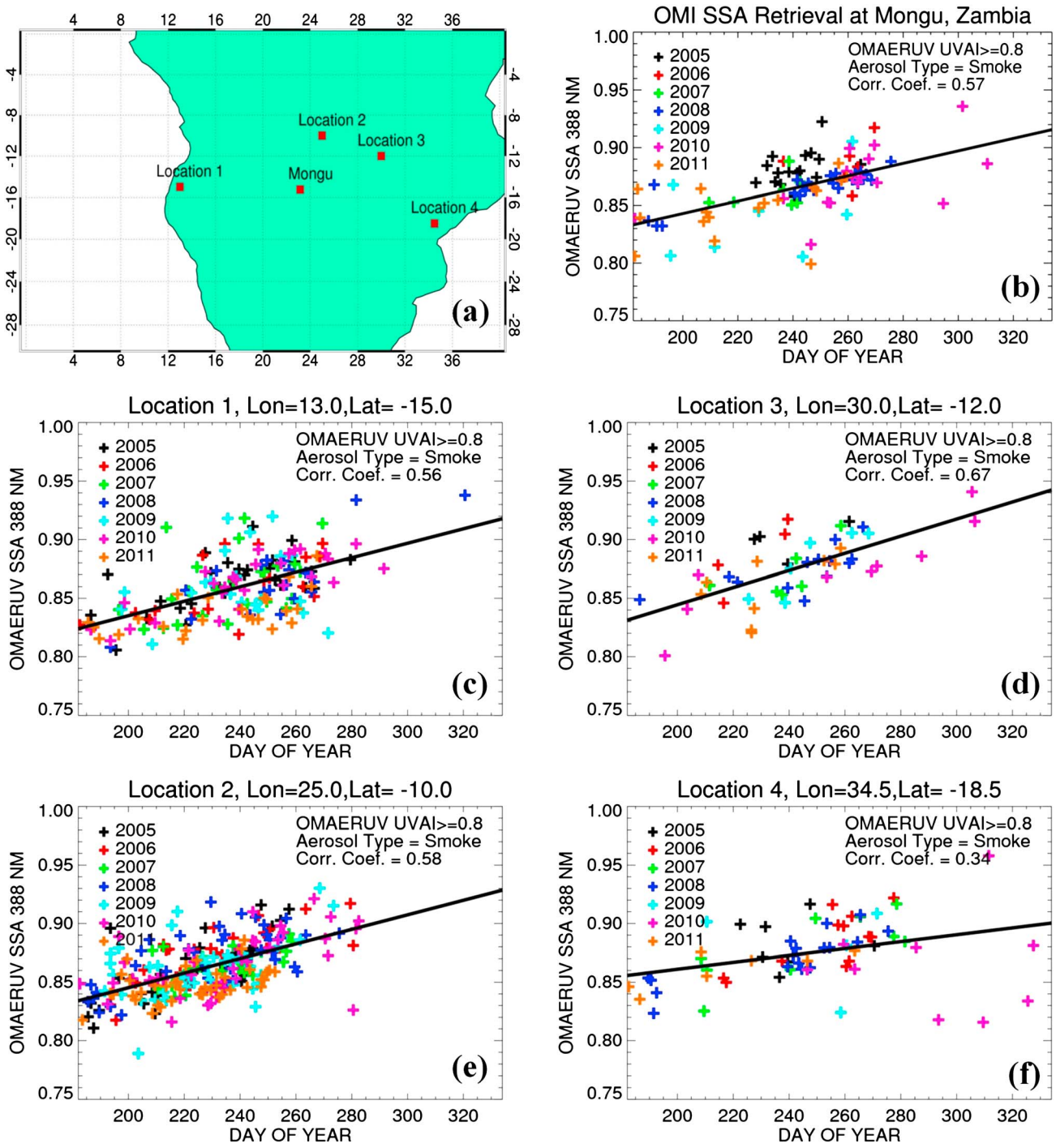

Figure 13. Biomass-burning season trends of SSA at 388 nm retrieved from OMI satellite data for Mongu, Zambia and four other selected sites in southern Africa.

Zambia that likely have higher AOD than further south due to the gradient of increasing biomass (potential fuel) to the north in this region. Site 4 is located near a newly established AERONET site in Gorongosa National Park in Mozambique. All four of these sites showed similar magnitude trends in SSA as was observed for the Mongu site location, although the trend was less coherent for Site 4 due to anomalously low SSA values late in the season for 1 year, 2010.

[29] Monthly maps of SSA at 388 nm from OMI for all of southern Africa (south of the equator) are shown in Figure 14. These maps are monthly means for the four primary burning season months of July to October computed from OMI data from the years 2004 to 2011. White areas on the maps are areas where the UV Aerosol Index was less than 0.8 due to insufficient aerosol signal resulting from a combination of low aerosol loading (AOD) and weak absorption. The maps depict a trend of increasing SSA from July to October throughout the vast majority of southern Africa. Therefore, these OMI retrieval maps suggest that the strong seasonal trends in SSA observed at the AERONET sites in

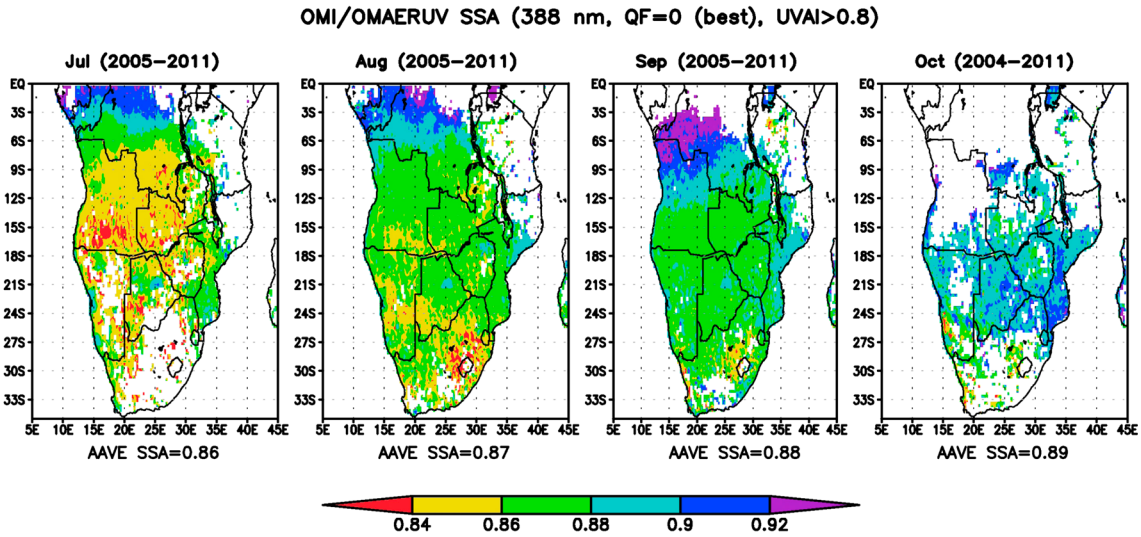

Figure 14. Monthly average maps of SSA at 388 nm retrieved from OMI for all of southern Africa for the principal biomass-burning season months of July to October.

Mongu and Etosha Pan are widespread throughout southern Africa in the biomass-burning season. This includes a strong seasonal trend of increasing SSA in the coastal region of Angola and Namibia adjacent to the extensive stratocumulus region in the southeast Atlantic, for which much recent analysis has been focused on the direct radiative forcing of the cloud/aerosol system [*Wilcox*, 2012; *Sakaeda et al*., 2011; *Chand et al*., 2009].

4. Discussion

[30] In the previous section, we have presented evidence of a seasonal shift in aerosol absorption throughout the burning season in southern Africa with the aerosol becoming increasingly more scattering (less absorbing) as the burning season progresses from July to October. Data measured both from AERONET ground-based monitoring sites and satellites were consistent in the general magnitude of this seasonal trend in absorption. In this section, we discuss patterns of biomass burning in southern Africa and suggest possible reasons for the observed trend in biomass-burning particle absorption. Additionally, we discuss the implications of this seasonal absorption trend for satellite remote sensing and on aerosol radiative forcing and inverted source function in the region.

4.1. Potential Causes of the Seasonal Absorption Trend

[31] MODIS maps of biomass-burning fire counts for southern Africa for both mid-July and mid-October in 2002 (Figure 15; http://rapidfire.sci.gsfc.nasa.gov/firemaps/) [*Davies et al*., 2004; *Giglio et al*., 2003b] show a significant seasonal shift in major burning regions mainly toward the east and south. The observed shift in regional biomass burning in 2002 is typical of other years as well. This shift suggests possible differences in fuel types (fraction of woody biomass, fuel moisture content) burned and also possible differences in transport time from the different burning regions to Zambia and or other parts of southern Africa. However, fire count numbers by themselves can be difficult to interpret in terms of smoke production, since one fire of woody fuels with high biomass content can produce much more aerosol than multiple fires with primarily grass fuels of much lower biomass content. Navigational errors coupled with uncertainty of the land surface properties can amplify this uncertainty [*Hyer and Reid*, 2009]. The lack of seasonal trends in fine-mode particle size at Mongu (Figures 8a and 8b) suggests that long distance transport does not result in significant particle modification, since aerosol aging typically results in growth in fine mode particle size from coagulation [*Colarco et al*., 2004; *Reid et al*., 1999] or growth from cloud interaction/processing. *Eck et al*. [2012] found no evidence of cloud processing in regions dominated by biomass-burning aerosols from AERONET retrievals.

[32] Since fuel moisture in southern Africa is likely to decrease as the dry season progresses with vegetation becoming increasingly senescent [*Justice et al*., 1996], woody fuels are more likely to burn in the late dry season when fuel moisture content is low enough. Although fire is an integral part of miombo woodland (the dominant tree species) ecology, human setting of fires is believed to have increased the frequency of fire far above the natural level. The wooded savanna in this region is typically incomplete canopy tree cover with under-canopy grass, making the discrimination from remote sensing of fuel type burned very difficult. Understory grasses may burn while the trees may not if the woody fuel moisture content is high enough. Much of the deliberate burning resulting in uncontrolled fires occurs at the end of the dry season, just before the onset of the summer rains. The fires burn with greater intensity as quantities of dry fuel accumulate [*Frost*, 1996]. These hotter fires are destructive even to fire-tolerant trees [*Chidumayo and Frost*, 1996]. Additionally, widespread regional burning consumes larger amounts of woody fuels as the dry season progresses with much of this consumption occurring through smoldering combustion of down woody fuels (limbs, tree trunks, stumps, etc.). These are fuels not involved in the early dry season fires, but which are consumed through mostly smoldering combustion later, and which continue to smolder until the rains set in.

[33] Chitemene is a form of slash-and-burn cultivation practiced in parts of this region. Although there are variations described by *Stromgaard* [1989], the basic form of

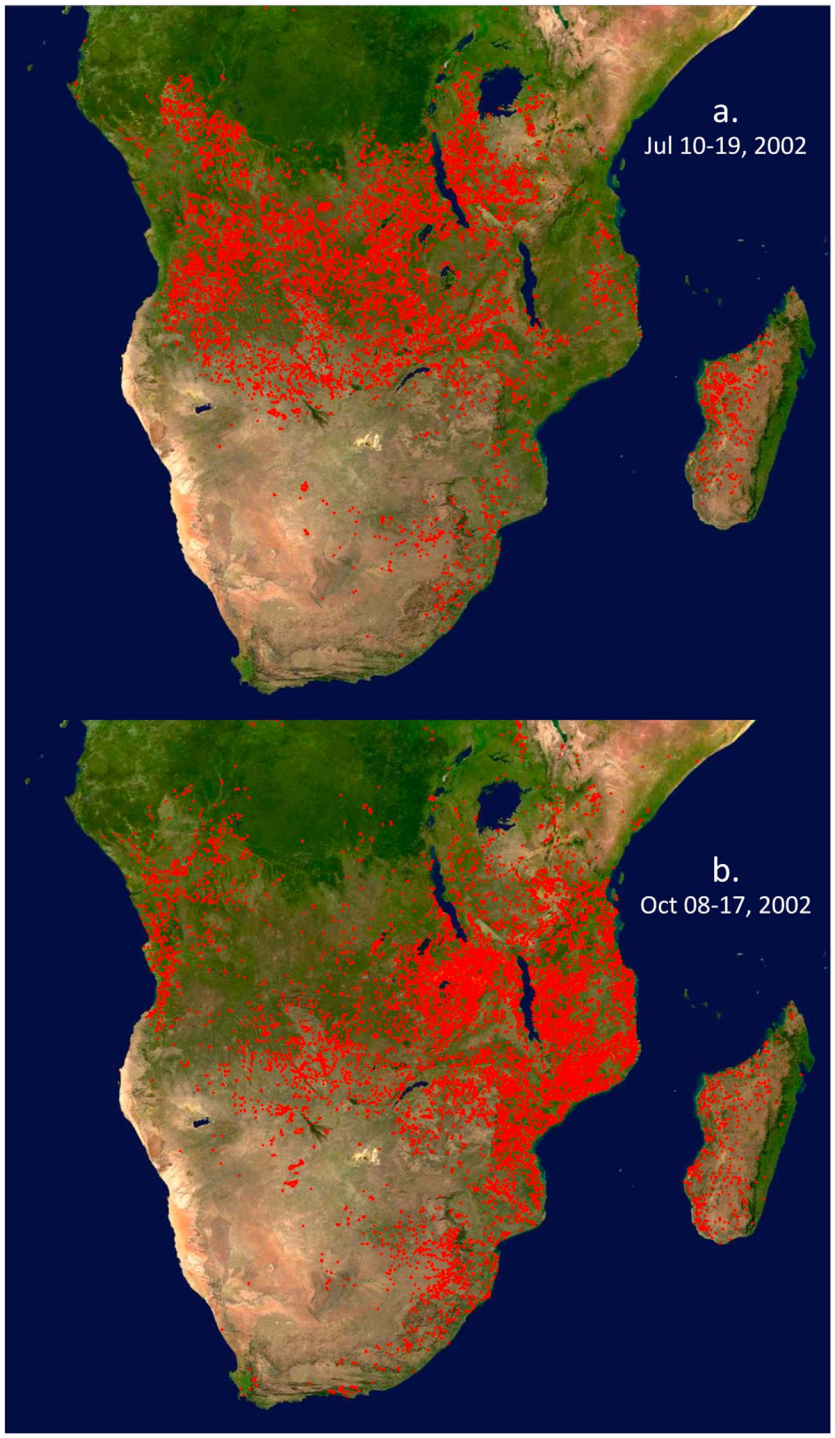

Figure 15. MODIS Fire counts (Terra + Aqua) for (a) 10–19 July 2002 and for (b) 8–17 October 2002.

chitemene is as follows. Branches are cut from trees within the selected area between July and September, laid out to dry, and before the beginning of the rains in November, are gathered into a pile in the middle of the cut area. The pile of branches is then burned just prior to the first rains, and crops are grown in the soil that has been fertilized by the ashes. Since woody fuels often burn with a higher percentage of smoldering phase combustion (versus flaming phase), these fires may produce smoke with less black carbon and higher SSA. However, chitemene fires often burn at high intensity with predominant flaming combustion although the fires often spread outside the intended burn area, and this combustion could have a higher smoldering component. The overall contribution of chitemene fires to black carbon production is therefore not clear.

[34] Conversely, at the beginning of the burning season in southern Africa, the fuels that are dry first and are most easily burned at that time are grasses, which tend to burn with a higher percentage of flaming phase combustion and thereby produce aerosols with higher black carbon content (more

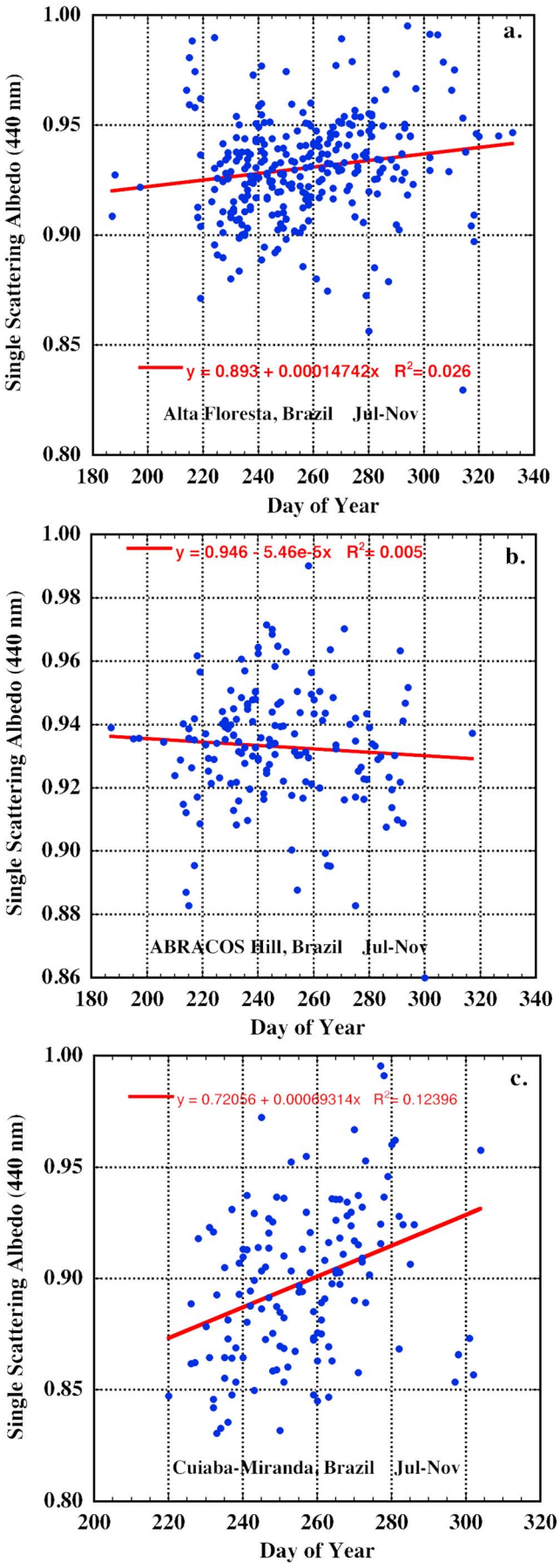

absorbing). As a result, the trends of increasing SSA as the burning season progresses as observed by both AERONET and OMI satellite data are likely to have been caused in part by a transition to increasing amounts of woody fuel combustion (and consequently more smoldering combustion) as the dry season progresses. However, it is beyond the scope of the available data and current analyses to conclusively confirm this or other factors as the cause of the observed trend in SSA in southern Africa.

[35] A comparison of seasonal smoke particle SSA trends in other tropical biomass-burning regions may also provide some insight on possible factors influencing the trends. Since the southern boundary of the Amazonian forest region has a strong biomass-burning season, during the same months as in southern Africa, we also examine the data from sites in this region. Data from three AERONET sites in Brazil, two in the Amazonia forest regions (Alta Floresta and Abracos Hill) where deforestation burns occur (in addition to pasture burns) and one in the cerrado region (woody savanna-like environment; CUIABA_MIRANDA site), were investigated with the same AOD and SZA thresholds (Level 2 data) thus ensuring consistency in data quality. The AERONET retrievals with the same processing algorithms, calibration methodology, and data quality checking [*Holben et al*., 2006] show a very different situation in the tropical forest region of South America versus the savanna environment of southern Africa. Figure 16 shows that there are no significant trends in SSA versus day of year in the two sites of the deforestation region (Alta Floresta and Abracos Hill), with the percentage of variance explained by the linear fit ranging from only 0.5% to 2.6%. This suggests that seasonal dynamic trends in burning differ significantly for these two major tropical biomass-burning regions. OMI retrievals of SSA at 388 nm for Alta Floresta show a similarly weak seasonality, with only a 0.02 increase in SSA from beginning to end of the burning season and linear correlation explaining only 2.8% of the variance. The lack of a trend in SSA observed from AERONET data for these multiyear analyses differs from that observed by *Rosário et al*. [2011] for the same forest burning region in Brazil. However, for the cerrado region site of CUIABA_MIRANDA, the AERONET data (1999–2011, but excluding the 2008 Level 2 data due to an instrument problem) do show a trend of increasing SSA as the burning season progresses, although much noisier (~12% of variance explained) than for the Mongu site. The OMI trend for this cerrado site also shows increasing SSA at 388 nm as the burning season progresses with 21% of variance explained, and a similar increase of ~0.06 over the burning season. This suggests that for the savanna-like environment of South America (cerrado), there may be a real tendency toward less absorbing aerosols at the end of the season, similar to that observed in the savanna environment of southern Africa, but much less coherent. The greater scatter in SSA at this cerrado site may be due in part to transport of forest burning smoke to the site from the Amazonia region to the north [*Eck et al*., 1998]. Since the

Figure 16. Time series of SSA (440 nm) from three AERONET sites in Brazil during the biomass-burning season months of July–October: (a) Alta Floresta, (b) Abracos Hill, and (c) CUIABA-MIRANDA.

trees are much larger in the Amazonia forest region than the savanna-woodlands of southern Africa, these larger woody fuels often do not completely burn in the first dry season after forest clearing. The larger tree trunks may take up to a few years longer to burn; therefore, subsequent burning years when pasture fires are used for agricultural land management may include smoldering combustion (less absorbing) from tree trunks still in the pastures in addition to the burning of pasture grass and/or shrubs. Therefore, differences in fuel types and mass (larger woody fuels in Amazonia) may be part of the reason for the lack of an observed trend in SSA in the biomass-burning AERONET sites in southern Amazonia.

4.2. Implications for Remote Sensing

[36] No doubt, a seasonally shifting single scattering albedo in such a high AOD environment will lead to nontrivial systematic biases in aerosol forcing estimates. For a unit optical depth, the migration of SSA at 550 nm from 0.81 at the beginning of July to 0.92 at the end of November (Figure 5) results in more than a factor of 2 difference in absorption optical depth. This trend is in part mitigated in studies that assume static SSA by choosing a mean value (reducing the absorption uncertainty to only 40%) as well as noting the highest AODs (and hence ultimate impact) are weighted toward the middle of the burning season, thus further cutting uncertainty. Given that the SSA in itself is not correlated to AOD (outside of the requirement that AOD > 0.4 for the retrieval), if one were to only consider absorption at the seasonal level, then the symmetric nature of the trend largely balances out. Possible interannual shifts in SSA, as demonstrated in Figure 3, perhaps pose a more worrying problem for climate scientists.

[37] The seasonal migration of regional single-scattering albedo in the southern African biomass-burning plume provides us with much needed microphysical information on the world's largest smoke feature, but also, perhaps even more importantly, an excellent natural laboratory on how the satellite sensor constellation interprets a large aerosol feature. While we examine this in this paper largely in the context of AOD, the same can be said for AAOD and top of atmosphere or estimated surface radiative flux.

[38] The systematic low bias in both standard operation MODIS and MISR products is likely associated with the overall low SSA in the southern African plume in comparison to other biomass-burning areas. For example, using AERONET retrievals similar to those used here, *Reid et al*. [2005b] over South America found the mean 440 nm SSA is on the order of 0.91 to 0.94 versus 0.88 for southern Africa. This is consistent with data shown in *Reid et al*. [2005a] of independent measurements of BC mass fraction that suggests a lower South American BC fraction compared to southern Africa. In the case of MODIS, the over land AOD retrieval assumes a static value of SSA of 0.85 at 550 nm in southern Africa [*Levy et al*., 2007a, 2007b]. This is only 0.01 lower than the average value found in our Figure 5. Now, *Hyer et al*. [2011] found that MODIS overall had a unity slope against AERONET over South America compared to 0.88 for southern Africa. This difference is certainly qualitatively consistent with the use of a static SSA retrieval coupled with the difference in observed SSA between the two biomass-burning regions. However, it is not definitive, as the SSA assumed in the MODIS retrieval for southern Africa is very close to the best estimate. There must be other components in the MODIS retrieval, which result in the overall low bias. This reason is not obvious to us, as the MODIS retrieval utilizes a real refractive index and size similar to what was found in AERONET retrievals from Mongu.

[39] To isolate the sensitivity in the retrieval to SSA versus other components in the optical model, we need only look to our finding that there was no detectable correlation to other retrieved microphysical parameters such as size or real refractive index. Similarly, the data assimilation product accounts for such things as seasonal varying surface albedo and viewing geometry (and an included static regional bias correction). With these findings and controls in place, the southern Africa biomass-burning plume provides a very rarely occurring natural partial derivative on how absorption influences our interpretation of satellite aerosol data. Our conclusion then is that the seasonal varying bias in MODIS AOD against AERONET is likely entirely related to SSA. This then suggests that other areas of the world with perhaps dynamic optical properties have built in microphysical bias which may be adding scatter to regression based verification studies.

[40] Finally, on the topic of satellite retrievals themselves, the results of this study clearly demonstrate the great potential of adding additional observational degrees of freedom to aerosol retrievals. We did not find any systematic or seasonal variability in MISR AOD retrieval error. In short, for the Mongu site, the MISR retrieval successfully controlled for varying absorption when all other things remain constant. The additional view angles and the associated complexity of the MISR over land retrieval resulted in a highly consistent (but 20% low biased) AOD product. Furthermore, examination of the large-scale verification of MISR [e.g., *Kahn et al*., 2010] shows that unlike MODIS, gain biases in MISR within biomass-burning regions do not appear to correlate with regional SSA, although some large site-specific biases exist. This finding is encouraging, in that it demonstrates that for good observing conditions, there is additional value provided by these retrieval technologies.

4.3. Implications for Data Assimilation and Inverse Modeling

[41] The satellite-AERONET comparison for the Mongu site represents an idealized case for demonstrating important factors for higher-order applications of satellite data such as data assimilation or inverse modeling. Overall, from a correlation and a root mean square deviation (i.e., removing the mean bias), Mongu is one of the top performing verification sites for MODIS and MISR. Cloud cover is limited and the cloud mask appears to work well. The overall coefficient of determination (r^2) is outstanding. However, even here, by performing multiyear analyses segregated by month in the MODIS data, we find even higher correlation subpopulations. Plus, the overall SSA for Mongu may vary systematically from year to year. Hence, these populations no doubt have a spatial and temporal correlation of their own which, in the absence of additional data, appears at first glance as "noise" in any long-term regression-based verification study. This finding is consistent with other findings such as from *Zhang and Reid et al*. [2009], *Hyer et al*. [2010], and *Shi et al*. [2011] that found large regions of spatially and temporally correlated bias over the globe related to such spatial

factors as lower boundary condition, aerosol type/microphysics, or the behavior of cloud masks. A key conclusion of these papers, and well demonstrated even with the individual comparisons done with the Mongu data set, is that the use of a uniform uncertainty for the MODIS product (or any current satellite aerosol product for that matter) is probably inappropriate for most scientific applications and the common assumption of observational errors being spatially uncorrelated is clearly not valid. Put another way, by and large satellite data users are treating systematic biases as random error, if it is even treated at all.

[42] The treatment of a collection of systematic biases as a "random error" has a number of important implications for data assimilation and inverse modeling. First, in the tradeoff between coverage and capability for data assimilation applications, the community tends to favor coverage as that is what is needed for consistent assimilation over a large area. Similarly, for inverse modeling of sources, the observations must be able to monitor the major features of the aerosol life cycle. Taking this further, for operational application, the community in general will trade capability for timeliness [*Reid et al*., 2011]. Hence, for these applications, products from lower fidelity sensors but with higher spatial/temporal coverage products such as MODIS or even geostationary will likely dominate data assimilation and inverse modeling applications. Given that the information content of the signal is insufficient to control microphysical degrees of freedom, one is left with little choice but to utilize larger observational errors, and this in return reduces the impact of the observations. Second, in the case of large-scale spatial variability in spatially/temporally correlated errors, regionally varying observation biases will result in discontinuities in data assimilation and will likely appear as artificial sources or sinks in the inverse model. On the other hand, if one has a more skillful retrieval, such as MISR, the bias is lower and less correlated, but it lacks the spatial coverage to adequately constrain the aerosol life cycle.

[43] The issues of correlated bias pose significant challenges for the community. However, one can view the case of southern Africa as an opportunity. Given that OMI data in Figure 14 suggest that SSA has a fairly large correlation length, one could theoretically use OMI or even monthly MISR data to better inform the MODIS retrieval. Similarly, if the source of the trend in SSA albedo can be fully resolved, models may be able to have some skill in predicting aerosol SSA. In either of these cases, southern Africa's seasonal "partial derivative" in SSA coupled with low cloud fraction and a significant number of smaller savanna fires, and considering its importance to global aerosol emissions may make it an ideal location to test multisensor algorithms or data assimilation technologies.

5. Summary and Conclusions

[44] We have analyzed the seasonal variation of aerosol absorption from both ground-based (AERONET) and satellite remote sensing retrievals (OMI) during the biomass-burning season in southern Africa. The principal findings and conclusions of this work are summarized as follows:

[45] 1. A strong seasonal trend of aerosol SSA has been observed from AERONET retrievals at sites in southern Africa from July to early November (biomass-burning season). At the Mongu, Zambia site, the SSA at 550 nm increased linearly by ~0.07 at 550 nm from July (~0.81 monthly mean) to October (~0.88). This is coincident with a significant linear decreasing trend in imaginary refractive index ($r^2 = 0.43$ at 440 nm), while aerosol size (accumulation mode dominated; seasonal average $\alpha_{440-870} = 1.85$) remained essentially constant with no significant trend ($r^2 < 0.02$) in either Ångström exponent or retrieved fine-mode particle radius. These data strongly suggest a change in aerosol composition during the burning season with a likely decreasing trend of black carbon percentage in the biomass-burning aerosol as the burning season progresses. Another site in southern Africa (Etosha Pan, Namibia) that is also dominated by biomass-burning aerosols showed very similar seasonal trends in both SSA and imaginary refractive index.

[46] 2. Comparison of MODIS retrievals of AOD versus AERONET measured AOD at Mongu, Zambia, shows that MODIS underestimates AOD to a greater extent in August as compared to September, and similarly greater underestimation in September versus October. This is consistent with the seasonal trend in SSA measured by AERONET since satellite retrievals of AOD are sensitive to assumed absorption magnitude, while the standard MODIS C5 algorithm assumes a constant value of SSA (0.85) throughout the year in this region for the retrieval of AOD. MISR retrievals of AOD do not appear to be impacted by the burning season trend in biomass-burning particles SSA, since these retrievals attempt to account for differences in absorption.

[47] 3. The aerosol single scattering albedo at 388 nm retrieved from multiyear OMI satellite measurements shows a similar seasonal trend as AERONET at Mongu, Zambia, and other locations in southern Africa. Monthly mean maps of SSA in Africa south of ~4°S show widespread seasonally increasing values of SSA from July to October, including the arid land areas that are immediately east of the persistent stratocumulus cloud deck in the southeast Atlantic. Therefore, it is highly likely that the biomass-burning aerosol that overlays this stratocumulus cloud layer also exhibits a seasonal trend in SSA during the burning season.

[48] Since neither the retrieved aerosol fine-mode radius nor the Ångström exponent showed any seasonal trend through the biomass-burning season months, it seems that aerosol aging and humidification/cloud processing can largely be ruled out as a cause of the trend in single scattering albedo, as these processes would result in increased fine-mode radius. However, the decrease in imaginary refractive index as the season progresses strongly suggests a change in aerosol black carbon content, which is possibly due to changes in types of fuel burned and the associated phase of combustion of these fuels. Throughout much of the region, much of the deliberate burning and the uncontrolled fires in woodlands occur at the end of the dry season, just before the onset of the summer rains. These fires burn with greater intensity as quantities of dry fuel accumulate and can be destructive even to fire-tolerant trees and also burn down woody fuels (branches, trunks, and stumps). Woody fuels burn with more smoldering phase combustion therefore produce smoke with less black carbon and higher SSA. Conversely, at the beginning of the burning season, the fuels that are dry first and are most easily burned at that time are grasses, which tend to burn with a higher percentage of

flaming phase combustion and thereby produce aerosols with higher black carbon content (more absorbing).

[49] **Acknowledgments.** The AERONET project was supported by Michael D. King, retired in 2008 from the NASA EOS project office, and subsequently by Hal B. Maring, Radiation Sciences Program, NASA Headquarters. We acknowledge Johan Le Roux of the Etosha Ecological Institute, Okuakuejo, Namibia, for the site management of the Etosha Pan AERONET site, and Bibi Bengis (South Africa National Parks) and Thomas Bigala for the site management of the Skukuza AERONET site.

References

Anderson, B. E., W. B. Grant, G. L. Gregory, E. V. Browell, J. E. Collins Jr., G. W. Sachse, D. R. Bagwell, C. H. Hudgins, D. R. Blake, and N. J. Blake (1996), Aerosols from biomass burning over the tropical south Atlantic region: Distributions and impacts, *J. Geophys. Res.*, *101*(D19), 24,117–24,137, doi:10.1029/96JD00717.

Bergstrom, R. W., P. B. Russell, and P. Hignett (2002), Wavelength dependence of the absorption of black carbon particles: Predictions and results from the TARFOX experiment and implications for the aerosol single scattering albedo, *J. Atmos. Sci.*, *59*, 567–577.

Bergstrom, R. W., P. Pilewskie, P. B. Russell, J. Redemann, T. C. Bond, P. K. Quinn, and B. Sierau (2007), Spectral absorption properties of atmospheric aerosols, *Atmos. Chem. Phys.*, *7*, 5937–5943.

Campbell, J. R., E. J. Welton, J. D. Spinhirne, Q. Ji, S.-C. Tsay, S. J. Piketh, M. Barenbrug, and B. N. Holben (2003), Micropulse lidar observations of tropospheric aerosols over northeastern South Africa during the ARREX and SAFARI 2000 dry season experiments, *J. Geophys. Res.*, *108*(D13), 8497, doi:10.1029/2002JD002563.

Chand, D., R. Wood, T. L. Anderson, S. K. Satheesh and R. J. Charlson (2009), Satellite-derived direct radiative effect of aerosols dependent on cloud cover, *Nat. Geosci.*, *2*, 181–184, doi:10.1038/NGEO437.

Chidumayo, E., and P. Frost 1996, Population biology of miombo trees in *The Miombo in Transition: Woodlands and Welfare in Africa*, edited by B. Campbell, pp. 59–71, CFIOR, Bogor, Indonesia.

Colarco, P. R., M. R. Schoeberl, B. G. Doddridge, L. T. Marufu, O. Torres, and E. J. Welton (2004), Transport of smoke from Canadian forest fires to the surface near Washington, D.C.: Injection height, entrainment, and optical properties, *J. Geophys. Res.*, *109*, D06203, doi:10.1029/2003JD004248.

Cooke, W. F., B. Koffi, and J.-M. Grégoire (1996), Seasonality of vegetation fires in Africa from remote sensing data and application to a global chemistry model, *J. Geophys. Res.*, *101*(D15), 21,051–21,065, doi:10.1029/96JD01835.

Crutzen, P. J., and M. O. Andreae 1990, Biomass burning in the tropics: Impacts on atmospheric chemistry and biogeochemical cycles. *Science 250*, 1669–1678.

Davies, D., S. Kumar, and J. Descloitres (2004), Global fire monitoring using MODIS near-real-time satellite data, *GIM International*, *18*(4), 41–43.

Diner, D. J. et al. (2010), MISR Level 2 Aerosol Retrieval Algorithm Theoretical Basis, JPL D-11400, Revision G. http://eospso.gsfc.nasa.gov/eos_homepage/for_scientists/atbd/docs/MISR/atbd-misr-09.pdf

Dubovik, O., and M. D. King (2000), A flexible inversion algorithm for the retrieval of aerosol optical properties from sun and sky radiance measurements, *J. Geophys. Res.*, *105*, 20673–20696.

Dubovik, O., A. Smirnov, B. N. Holben, M. D. King, Y. J. Kaufman, T. F. Eck, and I. Slutsker (2000), Accuracy assessments of aerosol optical properties retrieved from AERONET sun and sky-radiance measurements, *J. Geophys. Res.*,*105*, 9791–9806.

Dubovik, O., B. N. Holben, T. F. Eck, A. Smirnov, Y. J. Kaufman, M. D. King, D. Tanre, and I. Slutsker (2002), Variability of absorption and optical properties of key aerosol types observed in worldwide locations, *J. Atmos. Sci.*, *59*, 590–608.

Dubovik, O., et al. (2006), Application of spheroid models to account for aerosol particle nonsphericity in remote sensing of desert dust. *J. Geophys. Res.*, *111*, D11208, doi:10.1029/2005JD006619.

Eck, T. F., B. N. Holben, I. Slutsker, and A. Setzer (1998), Measurements of irradiance attenuation and estimation of aerosol single scattering albedo for biomass burning aerosols in Amazonia, *J. Geophys. Res.*, *103*, 31,865–31,878.

Eck, T. F., B. N. Holben, J. S. Reid, O. Dubovik, A. Smirnov, N. T. O'Neill, I. Slutsker, and S. Kinne (1999), Wavelength dependence of the optical depth of biomass burning, urban, and desert dust aerosols, *J. Geophys. Res.*, *104*, 31,333–31,349.

Eck, T. F., B. N. Holben, D. E. Ward, O. Dubovik, J. S. Reid, A. Smirnov, M. M. Mukelabai, N. C. Hsu, N. T. O'Neill, and I. Slutsker (2001), Characterization of the optical properties of biomass burning aerosols in Zambia during the 1997 ZIBBEE field campaign, *J. Geophys. Res.*, *106*, 3425–3448.

Eck, T. F., et al. (2003), Variability of biomass burning aerosol optical characteristics in southern Africa during the SAFARI 2000 dry season campaign and a comparison of single scattering albedo estimates from radiometric measurements, *J. Geophys. Res.*, *108*(D13), 8477, doi:10.1029/2002JD002321.

Eck, T. F., et al. (2008), Spatial and temporal variability of column-integrated aerosol optical properties in the southern Arabian Gulf and United Arab Emirates in summer, *J. Geophys. Res.*, *113*, D01204, doi:10.1029/2007JD008944.

Eck, T. F., et al. (2010), Climatological aspects of the optical properties of fine/coarse mode aerosol mixtures, *J. Geophys. Res.*, *115*, D19205, doi:10.1029/2010JD014002.

Eck, T. F., et al. (2012), Fog- and cloud-induced aerosol modification observed by the aerosol robotic network (AERONET), *J. Geophys. Res.*, *117*, D07206, doi:10.1029/2011JD016839.

Frost, P. (1996), The ecology of miombo woodlands. in *The Miombo in Transition: Woodlands and Welfare in Africa*, edited by B. Campbell, pp. 11–57, CFIOR, Bogor, Indonesia.

Garstang, M., P. D. Tyson, R. Swap, M. Edwards, P. Kållberg, and J. A. Lindesay (1996), Horizontal and vertical transport of air over southern Africa, *J. Geophys. Res.*, *101*(D19), 23,721–23,736, doi:10.1029/95JD00844.

Giglio, L., J. D. Kendall, and R. Mack (2003a), A multi-year active fire dataset for the tropics derived from the TRMM VIRS, *Int. J. Remote Sens. 24*, 4505–4525.

Giglio, L., J. Descloitres, C. O. Justice, and Y. J. Kaufman (2003b), An enhanced contextual fire detection algorithm for MODIS, *Remote Sens. Environ.*, *87*, 273–282, doi:10.1016/S0034-4257(03)00184-6.

Giglio, L., I. Csiszar, and C. O. Justice (2006), Global distribution and seasonality of active fires as observed with the Terra and Aqua MODIS sensors. *J. Geophys. Res. 111*, G02016. doi:10.1029/2005JG000142.

Giglio, L., J. T. Randerson, G. R. van der Werf, P. S. Kasibhatla, G. J. Collatz, D. C. Morton, and R. S. DeFries (2010), Assessing variability and long-term trends in burned area by merging multiple satellite fire products. *Biogeosci. 7*, 1171–1186. doi:10.5194/bg-7-1171-2010.

Giles, D. M., B. N. Holben, T. F. Eck, A. Sinyuk, A. Smirnov, I. Slutsker, R. R. Dickerson, A. M. Thompson, and J. S. Schafer (2012), An analysis of AERONET aerosol absorption properties and classifications representative of aerosol source regions, *J. Geophys. Res.*, *117*, D17203, doi:10.1029/2012JD018127.

Herman, J. R., P. K. Bhartia, O. Torres, C. Hsu, C. Seftor, and E. Celarier (1997), Global distribution of UV-absorbing aerosols from Nimbus 7/TOMS data, *J. Geophys. Res.*, *102*(D14), 16,911–16,922, doi:10.1029/96JD03680.

Holben, B.N., et al. (1998), AERONET—A federated instrument network and data archive for aerosol characterization, *Remote Sens. Environ.*, *66*, 1–16.

Holben, B. N., et al. (2001), An emerging ground-based aerosol climatology: Aerosol optical depth from AERONET, *J. Geophys. Res.*, *106*(D11), 12,067–12,097, doi:10.1029/2001JD900014.

Holben, B.N., T.F. Eck, I. Slutsker, A. Smirnov, A. Sinyuk, J. Schafer, D. Giles, and O. Dubovik (2006), AERONET's Version 2.0 quality assurance criteria, *Remote Sensing of Atmosphere and Clouds*, edited by Si-Chee Tsay, T. Nakajima, R.P. Singh, and R. Sridharan, Proc. SPIE Vol. *6408*, 64080Q, doi:10.1117/12.706524.

Holzer-Popp, T., et al. (2013) Aerosol retrieval experiments in the ESA aerosol_cci project, *Atmos. Meas. Tech. Discuss.*, *6*, 2353–2411, doi:10.5194/amtd-6-2353-2013

Hsu, N. C., J. R. Herman, P. K. Bhartia, C. J. Seftor, O. Torres, A. M. Thompson, J. F. Gleason, T. F. Eck, and B. N. Holben (1996), Detection of biomass burning smoke from TOMS measurements, *Geophys. Res. Lett.*, *23*(7), 745–748, doi:10.1029/96GL00455.

Hyer, E. J., and J. S. Reid (2009), Baseline uncertainties in biomass burning emission models resulting from spatial error in satellite active fire location data, *Geophys. Res. Lett.*, *36*, L05802, doi:10.1029/2008GL036767.

Hyer, E. J., J. S. Reid, and J. Zhang (2011), An over-land aerosol optical depth data set for data assimilation by filtering, correction, and aggregation of MODIS collection 5 optical depth retrievals, *Atmos. Meas. Tech.*, *4*, 379–408, doi:10.5194/amt-4-379-2011.

Ichoku, C., L. A. Remer, Y. J. Kaufman, R. Levy, D. A. Chu, D. Tanré, and B. N. Holben (2003), MODIS observation of aerosols and estimation of aerosol radiative forcing over southern Africa during SAFARI 2000, *J. Geophys. Res.*, *108*(D13), 8499, doi:10.1029/2002JD002366.

Intergovernmental Panel on Climate Change (IPCC) (2007), Climate change 2007: The physical science basis, in *Contribution of Working Group I to the Fourth Assessment Report of the Intergovernmental Panel on Climate Change*, edited by S. Solomon et al., 996 pp., Cambridge Univ. Press, Cambridge, U. K.

Jethva, H., and O. Torres (2011): Satellite-based evidence of wavelength-dependent aerosol absorption in biomass burning smoke inferred from ozone monitoring instrument, *Atmos. Chem. Phys.*, *11*, 10541–10551, doi:10.5194/acp-11-10541-2011.

Justice, C. O., J. D. Kendall, P. R. Dowty, and R. J. Scholes (1996), Satellite remote sensing of fires during the SAFARI campaign using NOAA advanced very high resolution radiometer data, *J. Geophys. Res.*, *101*(D19), 23,851–23,863, doi:10.1029/95JD00623.

Kahn, R. A., B. J. Gaitley, M. J. Garay, D. J. Diner, T. Eck, A. Smirnov, and B. N. Holben (2010), Multiangle imaging spectroradiometer global aerosol product assessment by comparison with the aerosol robotic network. *J. Geophys. Res. 115*, D23209, doi:10.1029/2010JD014601.

Leahy, L. V., T. L. Anderson, T. F. Eck, and R. W. Bergstrom (2007), A synthesis of single scattering albedo of biomass burning aerosol over southern Africa during SAFARI 2000, *Geophys. Res. Lett.*, *34*, L12814, doi:10.1029/2007GL029697.

Levelt, P. F., G. H. J. van den Oord, M. R. Dobber, A. Mälkki, H. Visser, J. de Vries, P. Stammes, J. O. V. Lundell, and H. Saari (2006), The Ozone Monitoring Instrument, IEEE Transactions on Geoscience and Remote Sensing, *44*(5), 1093–1101 doi:10.1109/TGRS.2006.872333.

Levy, R. C., L. A. Remer, S. Mattoo, E. F. Vermote, and Y. J. Kaufman (2007a), Second-generation operational algorithm: Retrieval of aerosol properties over land from inversion of moderate resolution imaging spectroradiometer spectral reflectance, *J. Geophys. Res.*, *112*, D13211, doi:10.1029/2006JD007811.

Levy, R. C., L. A. Remer, and O. Dubovik (2007b), Global aerosol optical properties and application to moderate resolution imaging spectroradiometer aerosol retrieval over land, *J. Geophys. Res.*, *112*, D13210, doi:10.1029/2006JD007815.

Lewis, K., W. P. Arnott, H. Moosmuller, and C. E. Wold (2008), Strong spectral variation of biomass smoke light absorption and single scattering albedo observed with a novel dual-wavelength photoacoustic instrument, *J. Geophys. Res.*, *113*, D16203, doi:10.1029/2007JD009699.

Lyapustin, A., et al. (2011), Reduction of aerosol absorption in Beijing since 2007 from MODIS and AERONET, *Geophys. Res. Lett.*, *38*, L10803, doi:10.1029/2011GL047306.

O'Neill, N. T., T. F. Eck, B. N. Holben, A. Smirnov, O. Dubovik, and A. Royer (2001), Bimodal size distribution influences on the variation of angstrom derivatives in spectral and optical depth space, *J. Geophys. Res.*, *106*, 9787–9806.

O'Neill, N. T., T. F. Eck, A. Smirnov, B.N. Holben, and S. Thulasiraman (2003), Spectral discrimination of coarse and fine mode optical depth, *J. Geophys. Res.*, *108*(D17), 4559, doi:10.1029/2002JD002975.

Piketh, S. J., H. J. Annegarn, and P. D. Tyson (1999), Lower tropospheric aerosol loadings over South Africa: The relative contribution of Aeolian dust, industrial emissions, and biomass burning, *J. Geophys. Res.*, *104*(D1), 1597–1607, doi:10.1029/1998JD100014.

Pilinis, C., S. N. Pandis, and J. H. Seinfeld (1995), Sensitivity of direct climate forcing by atmospheric aerosols to aerosol size and composition, *J. Geophys. Res.*, *100*(D9), 18,739–18,754, doi:10.1029/95JD02119.

Queface, A. J., S. J. Piketh, T. F. Eck, S-C. Tsay, and A. F. Mavume (2011), Climatology of aerosol optical properties in southern Africa, *Atmos. Environ.*, *45*(17), 2910–2921.

Reid, J. S. and P. V. Hobbs (1998), Physical and optical properties of young smoke from individual biomass fires in Brazil, *J. Geophys. Res.*, *103*(D24), 32,013–32,030, doi:10.1029/98JD00159.

Reid, J. S., T. F. Eck, S. A. Christopher, P. V. Hobbs, and B. N. Holben (1999), Use of the Ångstrom exponent to estimate the variability of optical and physical properties of aging smoke particles in Brazil, *J. Geophys. Res.*,*104*, 27,473–27,489.

Reid, J. S., T. F. Eck, S. A. Christopher, R. Koppmann, O. Dubovik, D. P. Eleuterio, B. N. Holben, E. A. Reid, and J. Zhang (2005a), A review of biomass burning emissions part III: Intensive optical properties of biomass burning particles, *Atmos. Chem. Phys.*, *5*, 827–849, doi:10.5194/acp-5-827-2005.

Reid, J. S., R. Koppmann, T. Eck, and D. Eleuterio (2005b), A review of biomass burning emissions part II: intensive physical properties of biomass burning particles, *Atmos. Chem. Phys.*, *5*, 799–825, SRef-ID: 1680-7324/acp/2005-5-799. http://www.atmos-chem-phys.org/acp/5/799/.

Reid, J. S., et al. (2009), Global monitoring and forecasting of biomass-burning smoke: Description and lessons from the fire locating and modeling of burning emissions (FLAMBE) program, *J of Sel. Topics in Appl. Earth Obs. and Rem. Sens*, *2*, 144–162.

Reid, J. S.; A. Benedetti, P. R. Colarco, and J. A. Hansen (2011), International operational aerosol observability workshop, *Bull. Am. Meteorol. Soc.*, *92*(6), Es21–Es24, doi:10.1175/2010bams3183.1.

Remer, L. A., et al. (2005), The MODIS aerosol algorithm, products, and validation, *J. Atmos. Sci.*, *62*(4), 947–973.

Robles-Gonzalez, C., and G. de Leeuw (2008), Aerosol properties over the SAFARI-2000 area retrieved from ATSR-2, *J. Geophys. Res.*, *113*, D05206, doi:10.1029/2007JD008636.

Rosário, N. E., M. A. Yamasoe, H. Brindley, T. F. Eck, and J. Schafer (2011), Downwelling solar irradiance in the biomass burning region of the southern Amazon: Dependence on aerosol intensive optical properties and role of water vapor, *J. Geophys. Res.*, *116*, D18304, doi:10.1029/2011JD015956.

Sakaeda, N., R. Wood, and P. J. Rasch (2011), Direct and semidirect aerosol effects of southern African biomass burning aerosol, *J. Geophys. Res.*, *116*, D12205, doi:10.1029/2010JD015540.

Schafer, J. S., T. F. Eck, B. N. Holben, P. Artaxo, and A. F. Duarte (2008), Characterization of the optical properties of atmospheric aerosols in Amazônia from long-term AERONET monitoring (1993–1995 and 1999–2006), *J. Geophys. Res.*, *113*, D04204, doi:10.1029/2007JD009319.

Schmid, B., J. Michalsky, R. Halthore, M.Beauharnois, L. Harrison, J. Livingston, P. Russell, B. Holben, T. Eck, and A. Smirnov (1999), Comparison of aerosol optical depth from four solar radiometers during the fall 1997 ARM intensive observation period, *Geophys. Res. Lett.*, *26*, 2725–2728.

Scholes, R. J., D. E. Ward, and C. O. Justice (1996), Emissions of trace gases and aerosol particles due to vegetation burning in Southern Hemisphere Africa, *J. Geophys. Res.*, *101*(D19), 23,677–23,682, doi:10.1029/95JD02049.

Shi, Y., J. Zhang, J. S. Reid, E. J. Hyer, T. F. Eck, B. N. Holben, and R. A. Kahn (2011), A critical examination of spatial biases between MODIS and MISR aerosol products—Application for potential AERONET deployment, *Atmos. Meas. Tech.*, *4*, 2823–2836, doi:10.5194/amt-4-2823-2011.

Smirnov, A., B. N. Holben, T. F. Eck, O. Dubovik, and I. Slutsker (2000), Cloud screening and quality control algorithms for the AERONET data base, *Remote Sens. Environ.*, *73*, 337–349.

Stromgaard, P. (1989), Adaptive strategies in the breakdown of shifting cultivation: The case of Mabwe, Lamba, and Lala of Northern Zambia. *Hum. Ecol. 17*, 427–444.

Swap, R. J., H. J. Annegarn, J. T. Suttles, M. D. King, S. Platnick, J. L. Privette, and R. J. Scholes (2003), Africa burning: A thematic analysis of the southern African regional science initiative (SAFARI 2000), *J. Geophys. Res.*, *108*(D13), 8465, doi:10.1029/2003JD003747.

Torres, O., P. K. Bhartia, J. R. Herman, Z. Ahmad, and J. Gleason (1998), Derivation of aerosol properties from satellite measurements of backscattered ultraviolet radiation: Theoretical basis, *J. Geophys. Res.*, *103*(D14), 17,099–17,110, doi:10.1029/98JD00900.

Torres, O., P. K. Bhartia, A. Sinyuk, E. J. Welton, and B. Holben (2005), Total ozone mapping spectrometer measurements of aerosol absorption from space: Comparison to SAFARI 2000 ground-based observations, *J. Geophys. Res.*, *110*, D10S18, doi:10.1029/2004JD004611.

Torres, O., A. Tanskanen, B. Veihelmann, C. Ahn, R. Braak, P. K. Bhartia, P. Veefkind, and P. Levelt (2007), Aerosols and surface UV products from ozone monitoring instrument observations: An overview, *J. Geophys. Res.*, *112*, D24S47, doi:10.1029/2007JD008809.

Torres, O., H. Jethva, and P. K. Bhartia (2012), Retrieval of aerosol optical depth above clouds from OMI observations: Sensitivity analysis and case studies. *J. Atmos. Sci.*, *69*, 1037–1053. doi:http://dx.doi.org/10.1175/JAS-D-11-0130.1

Ward, D. E., R. A. Susott, J. B. Kauffman, R. E. Babbitt, D. L. Cummings, B. Dias, B. N. Holben, Y. J. Kaufman, R. A. Rasmussen, and A. W. Setzer (1992), Smoke and fire characteristics for cerrado and deforestation burns in brazil: BASE-B experiment, *J. Geophys. Res.*, *97*(D13), 14,601–14,619, doi:10.1029/92JD01218.

Ward, D. E., W. M. Hao, R. A. Susott, R. E. Babbitt, R.W. Shea, J. B. Kaufman, and C. O. Justice (1996), Effect of fuel composition on combustion efficiency and emission factors for African savanna ecosystems, *J. Geophys. Res.*, *101*, 23569–23576.

van der Werf, G. R., J. T. Randerson, L. Giglio, G. J. Collatz, M. Mu, P. S. Kasibhatla, D. C. Morton, R. S. DeFries, Y. Jin, and T. T. van Leeuwen (2010), Global fire emissions and the contribution of deforestation, savanna, forest, agricultural, and peat fires (1997–2009). *Atmos. Chem. Phys. 10*, 11707–11735. doi:10.5194/acp-10-11707-2010.

Wilcox, E. M. (2012), Direct and semi-direct radiative forcing of smoke aerosols over clouds, *Atmos. Chem. Phys.*, *12*, 139–149, doi:10.5194/acp-12-139-2012.

Zhang, J., J. S. Reid, D. L. Westphal, N. L. Baker, and E. J. Hyer (2008), A system for operational aerosol optical depth data assimilation over global oceans, *J. Geophys. Res.*, *113*, D10208, doi:10.1029/2007JD009065.

Zhang, J., and J. S. Reid (2009), An analysis of clear sky and contextual biases using an operational over ocean MODIS aerosol product, *Geophys. Res. Lett*, *36*, L15824, doi:10.1029/2009GL038723.